

Lightweight, Practical Encrypted Face Recognition with GPU Support

Gabrielle De Micheli^{a,*}, Syed Mahbub Hafiz^{a,*}, Geovandro Pereira^{a,*}, Eduardo L. Cominetti^{a,*}, Thales B. Paiva^{a,b,*}, Jina Choi^c, Marcos A. Simplicio Jr^{a,b}, Bahattin Yildiz^a

^aAdvanced Security Team, LG Electronics, USA,

^bUniversidade de São Paulo, São Paulo, Brazil,

^cNext-Generation Computing Research Lab, CTO, LG Electronics, South Korea,

Abstract

Face recognition models commonly operate in a client-server setting where a client extracts a compact face embedding and a server performs similarity search over a template database. This raises privacy concerns, as facial data is highly sensitive. To provide cryptographic privacy guarantees, one can use fully homomorphic encryption (FHE) to perform end-to-end encrypted similarity search. However, existing FHE-based protocols are computationally costly and, especially, impose high memory overhead due to large rotation-key sets and bandwidth-bound homomorphic operations. Building on prior work, *HyDia*, we introduce algorithmic and system-level improvements targeting real-world deployment with resource-constrained (edge) clients. First, we propose BSGS-Diagonal, an algorithm delivering fast and memory-efficient similarity computation, benefiting from precomputed rotations when applying a Baby-Step/Giant-Step strategy to consecutive matrix-vector product evaluations. BSGS-Diagonal substantially shrinks the rotation-key set, lowering both client and server memory requirements, and also improves practical server runtime through upfront rotation reuse and a more parallel execution strategy. This yields a 91% reduction in the number of rotation keys, translating to approximately 14 GB less memory used on the client, and reducing overall CPU peak RAM from over 30 GB in the original *HyDia* to under 10 GB for databases up to size 2^{20} . In addition, runtime is improved by up to $1.57\times$ for the membership verification scenario and $1.43\times$ for the identification scenario. Secondly, we introduce fully GPU-optimized similarity matrix computation kernels, including an efficient Chebyshev evaluator. The implementation is built upon FIDESlib, a CKKS-level GPU library based on OpenFHE. Rather than offloading individual CKKS primitives in isolation, the integrated kernels fuse operations to avoid repeated CPU-GPU ciphertext movement and costly FIDESlib/OpenFHE data-structure conversions, which otherwise become dominant overheads and can make naive GPU execution no faster than a CPU-only implementation. As a result, our GPU implementations of both *HyDia* and BSGS-Diagonal achieve up to $9\times$ and $17\times$ speedups, respectively, enabling sub-second encrypted face recognition for databases up to 2^{15} entries while further reducing host memory usage.

Keywords: Facial Recognition, Privacy-Preserving Biometrics, Fully Homomorphic Encryption, CKKS

1. Introduction

Face recognition is the task of automatically verifying or identifying a person from an image (or video) of their face. It is increasingly being used across different domains such as healthcare, law enforcement or banking, in which the goal may be either membership verification (“is this person in the database?”) or identification (“which database entries match?”) [1]. In a typical client-server architecture, the client extracts

a real-valued compact face embedding from facial images using deep neural networks. The server then compares those embeddings against templates stored in a database, using a similarity metric (often, a cosine similarity).

Albeit simple, such common setups involving transmitting facial data to a remote server raises privacy concerns. Indeed, facial images are considered personally identifiable information (PII) and are subject to strict regulations on their usage and storage. This motivates the study and adoption of privacy-preserving face recognition approaches that limit identity leakage and protect against attempts to recover the original face from trans-

*Equal contribution from these authors.

Email address: gabrielle.demicheli@lge.com (Gabrielle De Micheli)

mitted data or intermediate representations (known as reconstruction attacks [2, 3, 4, 5]). One example is the deployment of transform-based techniques, where the client applies an irreversible transformation to the face image before it leaves the trusted device. This includes perturbation methods [6, 7, 8] or frequency-domain techniques [9, 10] to remove sensitive information while keeping relevant identity information. However, these transformations provide only empirical guarantees and can still leak identity information under strong recovery or adaptive attacks.

In light of these concerns, cryptographic schemes that enable matching directly on encrypted data represent a more robust alternative. Using techniques such as fully homomorphic encryption (FHE), garbled circuits, or multi-party computation (MPC), biometric data remains encrypted throughout the entire face recognition pipeline, as similarity computation is performed directly over ciphertexts. In this case, privacy assurance is derived from cryptographic security rather than obfuscation. Among these techniques, FHE is particularly attractive as it requires only a single round of communication between the client and the server, enabling more scalable and lower-latency architectures. Moreover, recent advances in software and hardware acceleration have significantly improved FHE’s practicality [11, 12], making it increasingly viable for real-time private face recognition.

Despite these advances, encrypted similarity search under FHE remains computationally demanding. For example, in CPU-based implementations of state-of-the-art schemes like CKKS [13], primary bottlenecks are ciphertext rotations, used in diagonal linear transforms and ciphertext-ciphertext multiplications, as well as rescaling operations required for similarity computation and threshold comparison. Profiling reveals that these CKKS operations are largely memory-bandwidth bound, making them promising candidates for GPU acceleration. However, naïvely offloading individual homomorphic operations to a GPU can degrade performance due to costly CPU–GPU ciphertext transfers, which may dominate overall latency unless the pipeline is carefully redesigned to minimize such communications.

In this work, we focus on an FHE-based face recognition protocol that supports both membership testing and identification scenarios, with particular emphasis on edge-device clients. Our design reflects realistic deployments in which the client is constrained in computation, memory, and energy, while the server has comparatively greater resources. The proposal builds upon the HyDia [14] protocol while addressing its main lim-

itation, which is also found in many FHE-based solutions: high RAM memory usage on both the client and server sides, largely due to the number of rotation keys that must be generated, transmitted, and stored. Our contributions include both algorithmic and system-wide improvements, described in what follows.

First, we incorporate a Baby-Step/Giant-Step (BSGS) strategy for the encrypted matrix–vector multiplication underlying the scheme’s similarity computation. Our variant, denoted BSGS-Diagonal, reduces computational overheads by precomputing and caching structured rotations before processing a sequence of similarity matrices, thereby significantly decreasing the rotation-key set. This results in 91% fewer rotation keys compared to HyDia, lowering client-side memory by approximately 14 GB and reducing overall peak RAM usage by up to $\approx 4.5\times$ for databases ranging from 2^{10} to 2^{20} entries. In addition to memory improvements, our BSGS variant is slightly faster than HyDia, reaching up to $1.57\times$ speedups.

As a second improvement, we design an end-to-end GPU-resident architecture for encrypted similarity search, addressing the computational bottlenecks of CPU-based FHE evaluation. Our approach follows a simple principle: upload the encrypted query once, execute similarity calculation, threshold comparison, and aggregation predominantly on the GPU, and minimize host–device transfers. We empirically validate this technique by integrating FIDESlib [12], a CUDA-accelerated CKKS library, with our OpenFHE-based framework. This integration includes a custom GPU-native Chebyshev evaluator, developed from scratch using the Paterson–Stockmeyer method, to avoid CPU round-trips for threshold comparison and ensure the entire pipeline remains GPU-resident. Our GPU implementation also incorporates deferred (lazy) relinearization in similarity accumulation and, for the BSGS path, pre-rotated diagonals with on-demand giant-step rotations. We provide GPU implementations for both the original HyDia and our BSGS variant, achieving up to $9\times$ and $17\times$ speedups, respectively. As a result, we reduce end-to-end runtimes to sub-second levels for databases up to 2^{15} entries. In addition to latency gains, GPU acceleration reduces host RAM usage by storing ciphertexts and intermediates on the GPU, further improving practicality for real-world deployments.

Our main contributions are summarized as follows:

1. Significant client- and server-side memory reduction for FHE-based face recognition, using an improved BSGS-style variant tailored for multi-similarity matrix computation, which low-

ers rotation-key requirements while yielding better performance.

2. To the best of our knowledge, the first GPU-accelerated implementation of an end-to-end encrypted face recognition protocol bringing membership and identification scenarios to sub-second execution time for databases of size up to 2^{15} . The acceleration comes from the introduction of new dedicated kernels with a custom comparison approach, in addition to a ciphertext multiplication kernel that avoids fused relinearization.
3. An open-source implementation based on OpenFHE [15] and FIDESlib [12] tested with databases of varying sizes up to 1M entries for CPU and 2^{16} entries for GPU. Our implementation code (CPU and GPU) can be found here: *to be added later*

Paper organization. Section 2 discusses related works on secure K -NN, private database search, secure facial recognition and GPU-based solutions. Section 3 reviews some important background material for our work, including the CKKS scheme, the diagonal and baby-step-giant-step method, the original HyDia [14], and security and privacy assumptions hereby considered. Section 4 presents our optimization proposal using of BSGS-Diagonal to replace HyDia’s diagonal method. Section 5 details our GPU-based implementation. Section 6 describes our experimental results, evaluating all the proposed optimizations. Finally, Section 7 presents our final considerations.

2. Related works

Secure K -NN. A core building block in similarity search is the K -nearest neighbors (K -NN) problem, sometimes also called top- K selection. Given a query vector, the K -NN problem identifies the K closest points in the dataset under a chosen metric (e.g., Euclidean distance, cosine similarity, or inner product). Many studies in the literature focus on secure K -NN schemes, using a variety of privacy preserving techniques to provide client’s query and/or database confidentiality. Early solutions [16, 17, 18, 19, 20] often combine HE with techniques such as MPC, oblivious RAM or garbled circuits. Most of these proposals suffer from significant practical limitations, such as long execution times, large communication complexity, access pattern leakage or multiple rounds of interaction with the client. Many subsequent works have focused on overcoming these

limitations. One example is the HE-based *approximate* classifier proposed by Shaul et al.[21], which provides an efficient solution to the *k-ish* NN problem. However, their implementation based on BGV [22] still takes several hours to run for medium-sized datasets. Later on, Chen et al. [23] introduced SANNS, two secure K -NN classifiers relying on homomorphic encryption, MPC, oblivious RAM and garbled circuits that keep both the client’s query and the search result confidential. As drawbacks, their solutions require asymptotically linear communication and are interactive, making them less suitable for outsourced computations. *Non-interactive* fully homomorphic K -NN algorithms also exist, such as the schemes by Zuber et al. [24] and Ameer et al. [25], both of which use TFHE [26] and have a quadratic cost in the size of the database. Without relying on HE, Servan-Schreiber et al. [27] presented PRECO, a first lightweight protocol for private nearest neighbor search where the server-side computation is efficient and the communication overhead is reduced to sublinear. PRECO relies on two non-colluding MPC servers running private NN searches, and achieves obliviousness by using distributed point functions, partial batch retrieval and oblivious masking. Finally, Cong et al. [28] focused on oblivious top- K selection, describing a TFHE-based non-interactive and secure K -NN classification with significant speedups compared to [24].

Private database search. While secure K -NN protocols address the problem of privately retrieving nearest neighbors, some works have explored private search in broader contexts. In these private search solutions, the goal is often to protect the client’s query itself, while the database may remain in plaintext in some scenarios. Ahmad et al. [29] presented Coeus, a private Wikipedia search system that uses BFV scheme [30] for the underlying homomorphic operations. The protocol relies on secure matrix-vector product using private information retrieval (PIR) and the Term Frequency-Inverse Document Frequency (TF-IDF) method [31] to protect the privacy of the users’ queries. Henzinger et al. [32] introduced Tiptoe, a private web search engine where clients can efficiently search over millions of public documents while protecting their queries. Tiptoe relies on semantic embeddings, private NN search with fast linearly homomorphic encryption (using BFV), and clustering to reduce communication. The server-side computational cost remains linear per query. More recently, Asi et al. [33] introduced Wally, another private search system which is efficient for very large databases and many clients. Wally relies both on Somewhat Homomorphic

Encryption (SHE) and differential privacy to guarantee the client’s query privacy. Concurrently to Wally, Zhou et al. [34] presented Pacmann, where clients run a graph-based approximate NN search combined with recent sublinear PIR schemes [35] to achieve better performance and accuracy than [32]. Focusing on a specific application, Wang et al. [36] presented PATHE, a privacy-preserving pattern search framework that integrates FHE (CKKS and TFHE) with hyperdimensional computing (HDC) to achieve high-performance secure mass spectrometry database search.

Graph-based similarity search. Other recent contributions have explored fully homomorphic encryption for encrypted search more broadly. Notably, the Graph-based Secure Similarity Search (GraSS) proposal [37] is a secure and scalable FHE-based framework for graph-structured similarity queries with end-to-end privacy. It defines an FHE-friendly graph representation and index encoding that reduces the complexity of neighborhood retrieval, including novel homomorphic algorithms tailored to graph operations. More recently, Zhu et al. [38] introduced Compass, a search system over encrypted embedding data. It uses a search index that includes the traversal of a graph-based ANN algorithm on top of Oblivious RAM for improved performance.

Privacy-preserving facial recognition. Bodetti [39] is one of the first studies on the practicality of using FHE for 1:1 private face recognition systems. The suggested algorithm relies on BFV and uses batching techniques for the homomorphic computation of inner products between vectors, so multiple elements are encrypted into a single encrypted block. In addition to these standard batching techniques, Bodetti also utilizes dimensionality reduction algorithms (in particular, the classical Principal Component Analysis) to further tackle the high computational cost of face matching over encrypted data.

Subsequently, Engelsma et al. [40] introduced a novel data encoding scheme that is tailored for efficient 1 : many representation matching in the encrypted domain, also using BFV. Compared to [39], their proposed HERS algorithm scales to larger databases due to a slower increase in computational complexity (namely, number of homomorphic additions and multiplications) and the absence of required rotations.

Later, Ibarrondo et al. [41] proposed replacing element-wise testing by the notion of group testing to significantly reduce the number of non-linear operations in the encrypted domain. More specifically, rather

than evaluating all scores individually, their proposed GROTE algorithm derives representative maxima for each group and performs threshold checks only on these values for better efficiency. Their algorithm relies on the CKKS homomorphic scheme.

Aiming to improve the efficiency of FHE-based face recognition, Choi et al. [42] proposed Blind-Match, a CKKS-based scheme where the feature vector is divided into smaller parts and each part is then processed individually. Their custom cosine similarity computation method allows them to reduce the number of additions and rotations compared to prior work [39] and outperform GROTE for varying database sizes.

More recently, Martin et al. [14] presented HyDia, another CKKS-based protocol for 1 : many face recognition that exploits diagonal packing for efficient matrix multiplication and scalability. The proposed algorithm uses a hybrid approximation method to compute homomorphic thresholding with better accuracy. Their study also provides a comprehensive comparison with the aforementioned works, including detailed plots and tables across multiple metrics such as server overhead, network bandwidth, circuit depth, and ciphertext size. Since HyDia is one of the latest works in private face recognition, and delivers state-of-the-art performance for large-scale 1 : many matching, we primarily compare our improvements to it, besides building upon their open-source implementation.

Another recent related work is CryptoFace [43], which targets an end-to-end setting where feature extraction itself is performed under FHE. The client encrypts the probe face image and the server evaluates an FHE-friendly convolutional neural network (CNN) to produce encrypted features for thresholded matching. Even though CryptoFace offers stronger protection by moving more of the pipeline into the encrypted domain, it is primarily evaluated for 1:1 verification, with identification demonstrated only via a small 1:128 closed-set retrieval experiment. In addition, its online latency is dominated by the homomorphic CNN feature-extraction stage (rather than by database-scale 1 : many matching), whereas HyDia and our work target and optimize the large-scale encrypted similarity search stage.

GPU-based similarity search. To the best of our knowledge, no public research articles report results specifically for GPU-accelerated encrypted face recognition. Nevertheless, public information on the topic can be found for CryptoLab’s Encrypted Facial Recognition (EFR) solution, described primarily through product and press material [44]. In those documents, the authors claim that GPU acceleration enables matching against

tens of millions of encrypted face-template vectors in milliseconds, with horizontal throughput scaling as additional GPUs are provisioned.

There are also many studies involving GPU acceleration for the FHE backend, rather than face-recognition applications directly. For example, the FIDESlib [12] library adopted in this work is an open-source, server-side CKKS-on-GPU library designed to interoperate with client-side OpenFHE workflows, including optimized GPU-oriented primitives and multi-GPU support. More broadly, proprietary and emerging libraries such as HEAAN2 [45] and Desilo [46] explicitly emphasize CUDA-based GPU acceleration for standard CKKS operations (e.g., rescaling, rotations/key-switching, and bootstrapping). Finally, the Cheddar GPU library [47] was very recently open-sourced. However, based on our initial investigation, it does not appear to provide support for encrypted matrix–vector multiplication. Therefore, a thorough analysis of its performance and eventual comparison with our FIDESlib-based implementation is left as a topic for future work.

3. Preliminaries

3.1. Mathematical notations

Throughout the paper, we will use a bold capital letter, say \mathbf{M} , to denote matrices and a bold letter, say \mathbf{q} , to denote a vector. We will use the \cdot notation for a standard matrix–vector multiplication operation and \odot to denote the element-wise multiplication operation.

3.2. CKKS

The CKKS scheme [13, 48] is a single instruction multiple data (SIMD)-style homomorphic encryption scheme that operates over a vector of complex or real values. The scheme relies on RingLWE ciphertexts in \mathcal{R}_Q^2 for a given ring $\mathcal{R} = \mathbb{Z}[X]/(X^N + 1)$, where $N = 2^k$ (for $k > 0$) is the ring dimension and $\mathcal{R}_Q = \mathcal{R}/Q\mathcal{R}$ describes the ring \mathcal{R} reduced modulo an integer $Q = \prod_{i=0}^L q_i$. The integer L is known as the *multiplicative depth* and represents the maximum number of rescaling levels available before decryption fails. CKKS supports element-wise operations, such as addition and multiplication, as well as cyclic rotation. We now describe some of the core operations supported by CKKS that are most relevant to this work.

Encoding. Given a real (or complex) vector $\mathbf{x} \in \mathbb{C}^{N/2}$, it is encoded into elements of \mathcal{R}_Q using an approximate inverse of a scaled complex canonical embedding. More precisely, one applies an inverse Fast Fourier Transform

on the elements of \mathbf{x} and scales each output by a factor Δ . Each element is then rounded to the nearest integer, since encryption is performed over integers modulo Q . This encoding step outputs a plaintext polynomial $\mathbf{m}(X)$ that packs $N/2$ complex values, referred to as the available *slots*.

Encryption. A plaintext polynomial $\mathbf{m}(X)$ is encrypted into a ciphertext $(\mathbf{a}, \mathbf{b}) \in \mathcal{R}_Q^2$ with a given public key and the addition of some random noise.

Addition. CKKS supports element-wise plaintext–ciphertext and ciphertext–ciphertext additions. The output ciphertext corresponds to the SIMD addition of the underlying complex vectors.

Multiplication. CKKS also supports plaintext–ciphertext and ciphertext–ciphertext multiplication. To avoid an exponential growth in the scaling factor over repeated multiplications, each multiplication is followed by a rescaling step. The output polynomial has coefficients in $\mathbb{Z}_{Q_{\ell-1}}$ instead of $\mathbb{Z}_{Q_{\ell}}$ where $Q_{\ell} = \prod_{i=0}^{\ell} q_i$ for $0 < \ell \leq L$. This corresponds to the consumption of one level from the available depth L .

Rotation. Cyclic rotations shift the elements of the input vector \mathbf{x} by $0 < k < N/2$ slots. The output ciphertext corresponds to the same underlying vector with shifted elements by k slots.

3.3. Diagonal method

The diagonal encoding method is a well-known technique for efficiently computing homomorphic matrix–vector products in a SIMD-friendly manner. Originally introduced by Halevi and Shoup [49, Section 4.3], the method starts by extracting the diagonals from a given matrix $\mathbf{M} \in \mathbb{R}^{\ell \times \ell}$ before computing the product homomorphically by summing rotated, element-wise products. More precisely, if $\text{diag}_i = (\mathbf{M}_{0,i}, \mathbf{M}_{1,i+1}, \dots, \mathbf{M}_{\ell-1,i-1})$ denotes the i th generalized diagonal of \mathbf{M} , then the product $\mathbf{M} \cdot \mathbf{v}$ is computed as

$$\mathbf{M} \cdot \mathbf{v} = \sum_{i=0}^{\ell-1} \text{Rot}_i(\mathbf{v}) \odot \text{diag}_i, \quad (1)$$

where Rot_i denotes a cyclic rotation by i slots and \odot denotes element-wise multiplication. In a standard plaintext–matrix setting, the vector \mathbf{v} is encrypted as a single ciphertext and each diagonal diag_i is a packed plaintext. The homomorphic evaluation involves, for each i , one ciphertext rotation, one plaintext–ciphertext multiplication, and one addition. Therefore, the method uses $\ell - 1$ rotations, ℓ multiplications, and $\ell - 1$ additions in total, i.e., the complexity is $O(\ell)$. Efficient implementations may take advantage of commonplace optimizations such as hoisting (see Section 3.4.2), but

those only affect constants underlying such asymptotic costs. The diagonal packing method also requires $\ell - 1$ (i.e., $\mathcal{O}(\ell)$ memory) rotation keys, which typically dominate the RAM footprint on both client and server sides.

We emphasize that Equation 1 describes the classical plaintext-matrix variant of the diagonal method, where the diagonals are known in advance and encoded as plaintext constants. In our setting, however, the database matrix is encrypted. This results in additional challenges, as further discussed in Section 3.4.1.

3.3.1. Diagonal method for rectangular matrices

In real-world applications, such as 1 : many facial matching scenarios, the matrix \mathbf{M} considered is not necessarily square. Indeed, standard face feature extractors [14, 50] often set the embedding vectors dimension ℓ to be a small power of two (e.g., FRGC2 dataset employs $\ell = 2^9$). On the other hand, facial template databases are often large, reaching a size K that may surpass 2^{20} entries. This unbalance between the parameters ℓ and K implies that Equation 1 cannot be directly applied to produce the desired K inner products.

We briefly recall how HyDia [14] approaches this problem via a packing strategy (see [14, Section 5.1] for additional details):

1. Consider a database DB containing K vectors of dimension ℓ , say $\text{DB} = \{v_0, \dots, v_{K-1}\}$. First, partition DB into groups of ℓ vectors, each one getting $\ell \times \ell$ square matrices S_j , for $0 \leq j < \lceil K/\ell \rceil$. The rows of matrix S_j will contain the vectors $v_{j\ell}, \dots, v_{(j+1)\ell-1}$.
2. For each square matrix \mathbf{S} , construct a diagonal matrix \mathbf{D} where the i -th diagonal entry is given by $\text{diag}_i(\mathbf{S}) = (\mathbf{S}_{0,i}, \mathbf{S}_{1,i+1}, \dots, \mathbf{S}_{\ell-1,i-1})$, for all i .
3. Since each CKKS ciphertext encodes `numSlots` coefficients, concatenate `numSlots`/ ℓ diagonal matrices horizontally. The resulting rectangular matrix is referred to in our work as \mathbf{M}_k , for $0 \leq k < G = \lceil K/\text{numSlots} \rceil$. Each row of \mathbf{M}_k is then encrypted into a separate ciphertext, yielding ℓ ciphertexts.
4. Repeat this process for all remaining diagonal matrices.

Figure 1 illustrates this process.

3.3.2. Packed matrices and batched multiplications

In the original diagonal method, the product $\mathbf{M} \cdot \mathbf{v}$ is defined for a single square matrix $\mathbf{M} \in \mathbb{R}^{\ell \times \ell}$ and a vector $\mathbf{v} \in \mathbb{R}^\ell$. In contrast, following HyDia, we leverage

the SIMD semantics of CKKS to batch multiple matrix-vector products. As explained in Section 3.3.1, we pack `numSlots`/ ℓ square matrices side-by-side into one enlarged representation. The query ciphertext employed follow a similar structure, carrying `numSlots`/ ℓ replicated copies of the same ℓ -dimensional query vector, aligned with the packed matrix blocks. The computation follows the diagonal method using component-wise (Hadamard) multiplication with rotations and slot-wise accumulations. Because all `numSlots`/ ℓ matrix blocks and replicated query vectors are packed via SIMD, the evaluation performs `numSlots`/ ℓ independent matrix-vector products in parallel. Hence, `numSlots`/ ℓ matrices are processed at essentially the cost of one matrix-vector multiplication.

3.4. Textbook Baby-step Giant-Step

The Baby-Step Giant-Step (BSGS) optimization reduces the number of ciphertext rotations needed in a homomorphic matrix-vector product by grouping the diagonals diag_i of \mathbf{M} into n_2 groups of size n_1 , such that $\ell = n_1 \cdot n_2$. By writing a diagonal index as $jn_1 + i$, with $0 \leq j < n_2$ and $0 \leq i < n_1$, the matrix-vector product given in Equation 1 can be re-indexed as

$$\mathbf{M} \cdot \mathbf{v} = \sum_{j=0}^{n_2-1} \sum_{i=0}^{n_1-1} \text{Rot}_{jn_1+i}(\mathbf{v}) \odot \text{diag}_{jn_1+i}(\mathbf{M}) \quad (2)$$

Note that Equation 2 still represents the fully unrolled diagonal method and, if evaluated directly, requires $\ell - 1$ ciphertext rotations. The actual BSGS gain appears after grouping the terms and using the following rotation identities: $\text{Rot}_{k+w}(\mathbf{a}) = \text{Rot}_k(\text{Rot}_w(\mathbf{a}))$, $\text{Rot}_k(\mathbf{a} \odot \mathbf{b}) = \text{Rot}_k(\mathbf{a}) \odot \text{Rot}_k(\mathbf{b})$, and $\text{Rot}_k(\mathbf{a}) \odot \mathbf{b} = \text{Rot}_k(\mathbf{a} \odot \text{Rot}_{-k}(\mathbf{b}))$. Factoring out $\text{Rot}_{jn_1}(\cdot)$ from Equation 2 gives

$$\begin{aligned} \mathbf{M} \cdot \mathbf{v} &= \sum_{j=0}^{n_2-1} \text{Rot}_{jn_1} \left(\sum_{i=0}^{n_1-1} \text{Rot}_i(\mathbf{v}) \odot \text{Rot}_{-jn_1}(\text{diag}_{jn_1+i}(\mathbf{M})) \right) \\ &= \sum_{j=0}^{n_2-1} \text{Rot}_{jn_1}(P_j) \end{aligned} \quad (3)$$

where the inner sum of products is defined as:

$$P_j := \sum_{i=0}^{n_1-1} \text{Rot}_i(\mathbf{v}) \odot \text{Rot}_{-jn_1}(\text{diag}_{jn_1+i}(\mathbf{M})).$$

Equation 2 can thus be rewritten as the following grouped matrix-vector multiplication:

$$\mathbf{M} \cdot \mathbf{v} = \sum_{j=0}^{n_2-1} \text{Rot}_{jn_1}(P_j). \quad (4)$$

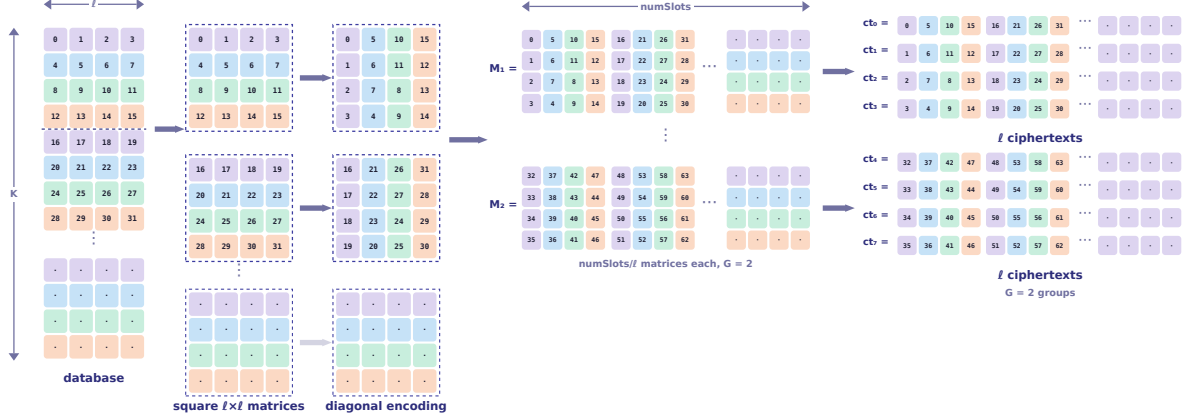


Figure 1: Pipeline showing the diagonal packing from HyDia generalized to multiple groups. When $K > \text{numSlots}$, more than one M_k matrix is produced (in this example, we have M_1 and M_2) to fit all the diagonal matrices. This results in $G \cdot \ell$ ciphertexts (in this figure, $\ell = 4$ and $G = 2$).

Equation 4 matches what was originally introduced in [51, Section 6.3].

A key observation is that the baby-step rotations $\text{Rot}_i(\mathbf{v})$, for $0 \leq i < n_1$, are shared across all groups P_j and therefore can be computed once and reused. As a result, the number of distinct ciphertext rotations drops from about $\ell - 1$ to $(n_1 - 1) + (n_2 - 1)$, namely the baby steps $1, \dots, n_1 - 1$ and the giant steps $n_1, 2n_1, \dots, (n_2 - 1)n_1$. This quantity is minimized when $n_1 \approx n_2 \approx \sqrt{\ell}$, yielding approximately $2\sqrt{\ell} - 2$ distinct rotations. Thus, the main advantages of BSGS is that it lowers the rotation cost from $O(\ell)$ to $O(\sqrt{\ell})$, together with a corresponding reduction in the number of rotation keys and the memory needed to store them. In the standard literature, this grouped form is especially useful when the matrix is in *plaintext* form. In that case, the rotated diagonals $\text{Rot}_{-j m_1}(\text{diag}_{j m_1 + i}(\mathbf{M}))$ can be pre-processed offline before the online homomorphic evaluation. Equivalently, one may view BSGS as using a table of baby-step rotations

$$\text{TB}[i] \leftarrow \text{Rot}_i(\mathbf{v}), \quad 0 \leq i < n_1,$$

which is computed once and reused across all giant-step groups. In the case of rectangular matrices, where Equation 4 is evaluated for many matrices M_k , the same baby-step table can be reused across all of them.

The number of homomorphic multiplications remains unchanged from the diagonal method, since each of the ℓ diagonals still contributes one product. Similarly, the number of homomorphic additions remains $\ell - 1$ because one must still combine all diagonal contributions. Thus, BSGS does not improve the asymptotic multipli-

cation complexity, which remains $O(\ell)$. Nevertheless, it does reduce the number of expensive ciphertext rotations and the associated key-storage cost.

3.4.1. Plaintext vs encrypted matrices

Most of the standard BSGS literature, including the grouped formulation given above, considers the setting where the matrix is in plaintext and only the input vector is encrypted. In that setup, the matrix diagonals are known in advance and can be pre-rotated, pre-encoded, and reused across many evaluations. The online computation therefore consists of ciphertext rotations applied to the encrypted query vector, followed by plaintext-ciphertext Hadamard products.

Conversely, the setting considered in this paper is different as the matrix itself is encrypted. Consequently, the usual plaintext-side preprocessing of diagonals is no longer available, and the online products are no longer plaintext-ciphertext but instead ciphertext-ciphertext. Therefore, the textbook grouped BSGS derivation above should be viewed as the reference BSGS construction from the standard literature, rather than as something that transfers directly to our setting. We define our own variant of grouped BSGS in Section 4.1, which we refer to as BSGS-Diagonal.

3.4.2. Hoisting and double hoisting for BSGS

Recall that, in Ring Learning With Errors (RLWE)-based schemes such as CKKS, a slot rotation by index k is implemented using a Galois automorphism σ_k on the ciphertext components, followed by a key-switching

operation that maps the secret key from $\sigma_k(\mathbf{sk})$ back to \mathbf{sk} .

A standard key-switch can be decomposed into two stages. The first stage is a ciphertext-dependent gadget decomposition $G_B(\mathbf{c})$ of the ciphertext \mathbf{c} into $\lceil \log_B(q) \rceil$ digits, where B is the gadget base and q is the current ciphertext modulus. The second stage is a ciphertext-independent accumulation that multiplies those digits by the corresponding rotation key and sums the result. Let C_1 denote the cost of the first stage and C_2 the cost of the second, where C_1 is usually significantly higher than C_2 in practice.

Hoisting applies whenever the same ciphertext is rotated by several indices $j \in \mathcal{J}$. In this case, instead of recomputing the gadget decomposition for every rotation, one computes $G_B(\mathbf{c})$ once and reuses it, reducing the cost from $|\mathcal{J}|(C_1 + C_2)$ to $C_1 + |\mathcal{J}|C_2$. In grouped BSGS, this applies directly to the baby-step rotations $\{\text{Rot}_i(\mathbf{c})\}_{i=0}^{n_1-1}$, since they all rotate the same input ciphertext \mathbf{c} . Hence, textbook BSGS is naturally *single-hoistable*.

Double hoisting, introduced by Bossuat et al. [52], is a further optimization on top of textbook BSGS. In the standard plaintext-matrix setting, it extends hoisting beyond the baby-step reuse and reduces the cost associated with the giant-step side of the computation.

In an encrypted-matrix setting, single hoisting still applies whenever the same ciphertext is rotated several times, since this only depends on reusing the ciphertext-dependent decomposition across multiple rotations. However, the standard double-hoisting optimization from the plaintext-matrix literature does not necessarily carry over. The reason is that the grouped products now involve encrypted matrix data rather than preprocessed plaintext diagonals, so the usual giant-step evaluation schedule and reuse pattern no longer apply. Any additional giant-step reuse beyond this would need to be specific to the chosen packing and evaluation order, rather than being directly taken from the textbook double-hoisted BSGS method for plaintext matrices. In our work, we propose a BSGS-style algorithm that supports double-hoisting in Section 4.1.

3.5. HyDia [14]

As a starting point to our work, we consider the HyDia protocol proposed in [14]. We refer to the actual paper for its technical details and hereby simply recall the main ideas behind HyDia, as that work serves as our main comparison point.

HyDia is a three-party protocol for one-to-many ($1 : K$) facial matching where both the query face embed-

ding and the database embeddings are encrypted end-to-end using CKKS. The scheme supports both membership verification and identification use cases. The overall system model can be described as follows. An enroller performs a one-time setup: it collects face images, runs a feature extractor to produce database template vectors (face embeddings), preprocesses them, encrypts them under a public key, and uploads the resulting template ciphertexts to the server’s database. The server stores the encrypted data and homomorphically evaluates client queries over it. The client captures a face image, derives a query template vector, preprocesses and encrypts it to form a query ciphertext, and asks whether the query matches any enrolled subject. The overall description of the protocol and the entities involved are illustrated in Figure 2.

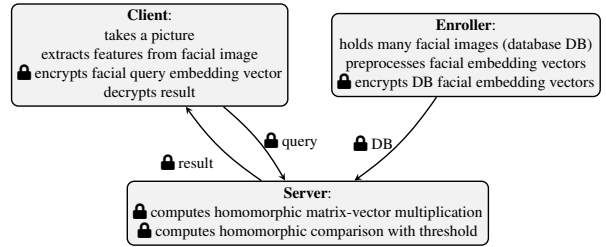


Figure 2: Illustration of the HyDia protocol (and ours).

One important characteristic of HyDia is that its design avoids revealing per-entry similarity scores. This prevents a semi-honest client from learning additional information about the database from their queries. This is accomplished by returning only a thresholded match decision or matching indices. In addition, HyDia outperforms methods proposed in prior works [41, 42, 40] by adapting diagonalized matrix multiplication to the $1 : K$ scenario, thus reducing expensive HE overhead and enabling higher parallelism. Moreover, the protocol supports single ciphertext queries (instead of sending hundreds of ciphertexts per query as in prior work), which significantly reduces communication and end-to-end latency. Finally, it uses a hybrid polynomial thresholding approximation that combines a lower depth Chebyshev approximation with a fixed polynomial degree (from Cheon et al. [53]), improving accuracy near the decision boundary without increasing the multiplicative depth budget.

3.6. Security and privacy assumptions

Entities to consider. Database search systems involve several key roles. The Client (C) submits queries and retains sole ownership of the decryption key. The Server

(**S**) stores the database and performs computations on encrypted data. In some scenarios, such as biometrics (for example in [41, 14]), an optional Enroller (**E**) is responsible for collecting plaintext samples and encrypting them immediately before transmitting them to the server. This ensures that only encrypted data is stored on the server to be compliant with privacy regulations such as GDPR and CCPA. Finally, an external attacker (**X**) models adversaries that can compromise **S** or the communication channels.

Privacy goals. Several privacy aspects must be preserved. Query privacy ensures that embeddings, biometric templates, or text queries remain secret. Database privacy prevents leakage of stored templates or embeddings, and result privacy restricts information revealed by similarity scores, indices, or top-K outputs for example. At a systems level, metadata privacy is also crucial to limit leakage through access patterns, timings, or ciphertext sizes. Finally, key confidentiality requires that only trusted entities hold decryption keys (typically the client).

Assumptions. Standard security assumptions vary by role. The server is usually considered semi-honest in FHE settings. The client is also considered semi-honest in FHE but may behave maliciously in differential privacy or anonymity-based protocols [33]. The enroller is trusted and assumed not to collude with **S** or **C** [14].

System states. Depending on the application, the database and queries nature can vary. Databases may be encrypted at rest by the enroller (for biometrics [39, 41, 14, 40]), public (in the setting of anonymous search [33]), or consist of encrypted embeddings/documents (encrypted RAG [54]). Queries may be fully encrypted under the client’s key, anonymized with differential privacy padding, or encrypted before leaving the client device.

Face recognition scenario. In FHE-based face recognition, the database is encrypted by the enroller and stored at the server. Queries are encrypted by the client, and the server only evaluates over ciphertexts. The client decrypts results and learns only the indices of matches, while the enroller is trusted only at enrollment.

Our threat model. In our work, we closely follow the threat model given in [14] as we build upon their work and specifically consider face-recognition scenarios. The client and the server in our system are semi-honest. The security of our protocol relies on the security of the CKKS scheme, which is based on the hardness of the Ring Learning with Errors problem. Note

Layout parameters	
K	Total number of database vectors.
ℓ	Vector dimension of each database/query vector.
numSlots	CKKS batch size (number of SIMD slots).
$G = \lceil \frac{K}{\text{numSlots}} \rceil$	Number of groups (each containing up to $\lceil \text{numSlots}/\ell \rceil$ square diagonal matrices).
BSGS parameters	
n_1	Baby-step size
n_2	Giant-step size ($n_2 = \lceil \ell/n_1 \rceil$).
Similarity computation parameters	
\mathbf{M}_k	Concatenation of $\text{numSlots}/\ell$ square diagonal matrices in encrypted form
\mathbf{q}	Encrypted query vector (single ciphertext).
$\text{diag}_i(\mathbf{M}_k)$	i^{th} diagonal ciphertext of matrix \mathbf{M}_k
κ	Comparative depth budget
GPU parameters	
$\text{diag}'[k]$	Pre-rotated diagonal ciphertext, $\text{diag}'[k] = \text{Rot}_{-\lfloor k/n_1 \rfloor n_1}(\text{diag}[\mathbf{M}_k])$.
n	Chebyshev poly degree (e.g., $n=13$ for $\kappa=8$).
S	CUDA stream pool size (Equation 6).
SMs	GPU streaming multiprocessor count.
F	Free GPU memory (bytes).
C	Estimated per-ciphertext size on GPU.

Table 1: Parameters and variables used in the diagonal BSGS enrollment and query processing.

that CKKS provides post-quantum security for an appropriate choice of encryption parameters.

3.7. Summary of parameters involved

We summarize the main parameters used in our algorithms and pseudo-codes in Table 1.

4. Improved HyDia with BSGS Key Reduction

One way of improving HyDia’s diagonal encoding method [14] is integrating a BSGS algorithm to reduce the number of rotation keys generated and transmitted by the client and processed by the server. This greatly lowers RAM requirements while improving performance. This improvement specifically targets the homomorphic similarity computation that happens on the server side for both membership and identification scenarios.

4.1. BSGS with precomputation across groups

In this section, we present an optimized BSGS-style algorithm for our encrypted matrix setting, which we call BSGS-Diagonal. Unlike the textbook BSGS method, which is typically described for plaintext matrices and exploits grouped giant steps together with plaintext diagonal preprocessing, our setting works with encrypted matrix groups \mathbf{M}_k . The main idea of BSGS-Diagonal is therefore different. Instead of relying on the usual plaintext-side giant-step reuse, we precompute

the required rotations of the encrypted query once and reuse them across all matrix groups. We additionally introduce an improved threaded evaluation strategy to reduce the RAM overhead of this precomputation.

Recall from Section 3.3.1 that when the number of database vectors K exceeds the packing capacity, the database is partitioned into multiple encrypted matrix groups \mathbf{M}_k , for $0 \leq k < G$, and the server must evaluate G matrix-vector products $\mathbf{M}_k \cdot \mathbf{q}$, where \mathbf{q} is the query ciphertext produced by the client. In the standard grouped BSGS formulation, each group would be evaluated using grouped baby-step and giant-step rotations. However, since the same query ciphertext \mathbf{q} is used for all groups, the full set of query rotations needed across all \mathbf{M}_k can instead be generated once and reused throughout the entire computation.

More precisely, rather than evaluating each group through the grouped form of Equation 4, we use the unrolled diagonal expression

$$\mathbf{M}_k \cdot \mathbf{q} = \sum_{i=0}^{\ell-1} \text{rotQ}[i] \odot \text{diag}_i(\mathbf{M}_k), \quad (5)$$

for $0 \leq k < G$, where $\text{rotQ}[i] \leftarrow \text{Rot}_r(\mathbf{q})$. Thus, rotQ is a table containing all ℓ rotated versions of the query ciphertext required by the diagonal decomposition. The main advantage is that this table is computed once and then reused across all G encrypted matrix groups.

This changes the role of BSGS in our setting. In the plaintext-matrix literature, BSGS reduces the number of distinct online rotation offsets by grouping terms into baby steps and giant steps. In our encrypted-matrix case, the main benefit comes instead from amortizing the cost of query rotations across many groups. Once the table `rotatedQuery` has been generated, no further query rotations are needed while processing the remaining matrix groups. Hence, the rotation cost associated with the query no longer scales linearly with the number of groups G , but is paid once and then reused.

The precomputation of `rotatedQuery` can itself exploit hoisting, since all required rotations are applied to the same input ciphertext \mathbf{q} . Therefore, the ciphertext-dependent decomposition of \mathbf{q} can be shared across the rotations used to build the table. We emphasize, however, that this is different from the textbook double-hoisted BSGS method for plaintext matrices. In our setting the matrices \mathbf{M}_k are encrypted, so the usual plaintext-diagonal preprocessing and giant-step reuse pattern from the standard double-hoisting literature does not apply. We thus view BSGS-Diagonal as a BSGS-inspired precomputation method for encrypted matrices,

rather than as a direct instance of the standard double-hoisted BSGS algorithm.

The tradeoff is that BSGS-Diagonal stores more rotated query ciphertexts simultaneously in memory, since the table `rotatedQuery` contains ℓ ciphertexts. In return, it removes the need to recompute or re-rotate the query for every group, which yields a substantial reduction in total runtime when the number of groups G is large. In addition, the relinearizations of the accumulated sums of ciphertexts can be postponed to the very end when evaluating Equation 5, as no intermediate rotation is applied in the process. A single relinearization is applied per matrix group. In comparison to a textbook BSGS approach, n_2 relinearizations have to be performed per group (Equation 4), since before each giant rotation by jn_1 the input ciphertext is recommended to be relinearized to avoid memory explosion issues¹. Moreover, to mitigate the additional memory overhead, we also introduce a memory-aware multi-threaded processing strategy that limits the number of temporary ciphertexts kept live during evaluation.

Memory-Efficient Accumulation. When generating the partial products in Equation 5 in a multi-threaded implementation *incremental accumulation* can be used for RAM memory reduction. For each matrix group, we compute all ℓ ciphertext products and store them before summing:

$$\text{products}[i] \leftarrow \text{rotQ}[i] \odot \text{diag}_i(\mathbf{M}_k).$$

This requires $O(\ell)$ ciphertext storage simultaneously, which for $\ell = 512$ and ciphertext size ≈ 8 MB amounts to approximately 4 GB per matrix group.

On a multi-core processor BSGS-Diagonal can be adapted to employ a per-thread running accumulators:

$$\text{accumulator}_t += \text{rotQ}[i] \odot \text{diag}_i(\mathbf{M}_k)$$

where products are added to thread-local accumulators immediately after computation and then freed. With T threads, memory consumption drops from $O(\ell)$ to $O(T)$ ciphertexts, reducing peak RAM from ≈ 4 GB to $\approx T \times 8$ MB per matrix group. The full version of BSGS-Diagonal with multi-threading processing is illustrated by Algorithm 1.

As our optimizations focus on the computation of the homomorphic inner product itself, our new algorithm

¹OpenFHE for example does not implement rotation operation on quadratic or higher degree ciphertext due to the memory issue. <https://openfhe.discourse.group/t/which-operations-can-be-followed-multiplication-w-o-relinearization/1148>

Algorithm 1 BSGS-Diagonal: BSGS variant with Incremental Accumulation

Require: Query ciphertext \mathbf{q} , database diagonal ciphertexts
Ensure: Similarity scores for all database vectors

```
1:  $\triangleright$  Step 1: Baby-step rotations with hoisting
2: queryPre  $\leftarrow$  rotPrecompute( $\mathbf{q}$ )
3: for  $b = 0$  to  $n_1 - 1$  in parallel do
4:   rotQ[b]  $\leftarrow$  hoistedRot( $\mathbf{q}, b, \text{queryPre}$ )
5: end for

6:  $\triangleright$  Step 2: Double hoisting - precompute for giant steps
7: for  $b = 0$  to  $n_1 - 1$  in parallel do
8:   babyPre[b]  $\leftarrow$  rotPrecompute(rotQ[b])
9: end for

10:  $\triangleright$  Step 3: Compute all rotations upfront
11: for  $i = n_1$  to  $\ell - 1$  in parallel do
12:    $(b_1, b_2) \leftarrow (i/n_1, i \bmod n_1)$ 
13:   rotQ[i]  $\leftarrow$  hoistedRot(rotQ[b2],  $b_1 \cdot n_1, \text{babyPre}[b_2]$ )
14: end for

15:  $\triangleright$  Step 4: Process groups with incremental accumulation
16: for each matrix group  $\mathbf{M}_k$  do
17:   Initialize per-thread accumulators  $\text{acc}_t \leftarrow \mathbf{0}$ 
18:   for  $i = 0$  to  $\ell - 1$  in parallel do
19:     prod  $\leftarrow$  rotQ[i]  $\odot$  diag( $\mathbf{M}_k$ )  $\triangleright$  No relinearization
20:      $\text{acc}_t \leftarrow \text{acc}_t + \text{prod}$   $\triangleright$  Free product immediately
21:   end for
22:   result[k]  $\leftarrow$  TreeReduce( $\text{acc}_0, \dots, \text{acc}_{T-1}$ )
23:   result[k]  $\leftarrow$  Relinearize(result[k])
24: end for

25: return result
```

can easily substitute the diagonal method used by the server in HyDia. The membership and index scenarios remain the same as in the original HyDia paper and we recall their pseudo-code in Algorithms 7 and 8 in Appendix B.

4.2. Complexity analysis and memory consumption

4.2.1. Complexity analysis for HyDia

We briefly recall the complexity of the HyDia algorithm to compare with our new variant in terms of performance, error growth and memory consumption. We refer to [14, Appendix E] for details but recall here the algorithmic complexity to compute the encrypted similarity on the server side. Let G denote the number of groups of ℓ ciphertexts, K the number of database vectors and ℓ the dimension of those vector embeddings, then HyDia’s algorithm will require $G \cdot (\ell - 1)$ ciphertext-ciphertext additions, $G \cdot \ell$ ciphertext-ciphertext multiplications, G relinearizations and rescaling and $\ell - 1$ hoisted rotations.

4.2.2. Complexity analysis of our BSGS-Diagonal

The BSGS-Diagonal algorithm requires $G \cdot (\ell - 1)$ ciphertext-ciphertext additions, $G \cdot \ell$ ciphertext-ciphertext multiplications, G relinearizations, G rescalings and $(\ell - 1)$ hoisted rotations. Note that while BSGS-Diagonal saves a factor G number of rotations when compared to the textbook BSGS (Equation 2), it requires the same operation counts as the original HyDia diagonal method, while saving a significant amount of memory.

Remark 1. *There is a tradeoff between BSGS-Diagonal and a single-hoisted grouped BSGS strategy, depending on the database size and hence on the number of matrix groups G . For small G , the single-hoisted grouped BSGS approach is often preferable. It performs fewer total query rotations and stores fewer rotated ciphertexts in memory. By contrast, when G becomes sufficiently large, BSGS-Diagonal becomes more time-efficient because the cost of query rotations is paid once upfront and then amortized across all groups.*

More precisely, the total number of nontrivial query rotations is $(n_1 - 1) + G(n_2 - 1)$ for the single-hoisted grouped BSGS approach, whereas for BSGS-Diagonal it is $n_1 n_2 - 1$. Thus, BSGS-Diagonal becomes advantageous when the number of groups G is large enough that recomputing giant-step rotations across groups is more expensive than precomputing the full table of rotated queries once.

The tradeoff is in the memory cost. Single-hoisted grouped BSGS stores about n_1 rotated query ciphertexts, whereas BSGS-Diagonal stores the full table of $\ell = n_1 n_2$ rotated query ciphertexts. Hence BSGS-Diagonal uses approximately $\ell - n_1$ additional ciphertexts in memory. In our experiments, we observed that for database sizes up to 2^{18} , the single-hoisted grouped BSGS approach is preferable, while for database sizes 2^{19} and above, BSGS-Diagonal becomes more time-efficient. For databases with about one million entries, it already reduces the query-rotation count by roughly a factor of 3 under our parameter setting. Table A.4 in Appendix B summarizes this tradeoff for the CKKS parameters used in our implementation.

4.2.3. Lowering the RAM consumption

Client-side. We compare the number of rotation keys that the client need to generate for both the diagonal method in HyDia and our BSGS variant. We start by counting the number of rotation keys required by the HyDia protocol. To support the within-block diagonal

matrix–vector multiplication, one requires $\ell-1$ rotations $\{1, 2, \dots, \ell-1\}$.

On the other side, our BSGS-Diagonal variant only requires a set of rotation keys for both the baby steps S_{baby} and giant steps S_{giant} with $S_{baby} = \{1, 2, \dots, n_1 - 1\}$, and $S_{giant} = \{(jn_1) : 1 \leq j < n_2\}$. We will show in Section 6.3 that for the parameters chosen for both HyDia and our BSGS-Diagonal, this corresponds to a significant reduction in the amount of rotation keys required to be generated by the client.

5. GPU-accelerated encrypted search

The CPU-based similarity computation described in Section 4 is bottlenecked by two classes of operations: (i) ciphertext rotations during the diagonal linear transform and (ii) ciphertext–ciphertext multiplications, re-linearization, and rescaling during both the similarity computation and the Chebyshev comparison. Profiling of the CPU implementation reveals that the homomorphic matrix–vector product (rotations, multiplications, and accumulations) dominates per-query time, while the individual HE operations—multiplication, addition, rescaling—are limited by memory bandwidth rather than arithmetic throughput, precisely the regime where GPU acceleration is most effective.

Note that a naive approach of offloading individual HE operations to the GPU, however, can be *slower* than the CPU. The reason is that each ciphertext must be converted between the host CPU (OpenFHE [15]) and device GPU (FIDESlib [12]) data structure representations, a process that can cost tens to hundreds of milliseconds per ciphertext depending on the CKKS parameter set—comparable to the cost of several ciphertext rotations in GPU. Any strategy that uploads and downloads intermediate results after each operation, therefore, incurs a transfer overhead that dominates the compute savings. Our GPU design is therefore guided by a single principle: *minimize host–device transfers by keeping the entire query processing pipeline on the GPU*, i.e., uploading only the query ciphertext and downloading only the final encrypted score comparison result.

In this section, we describe how the two CPU variants considered—the original diagonal method HyDia and a textbook BSGS—are ported to the GPU following the above principle, namely, HyDia-GPU-DG and BSGS-GPU-PRS. The two variants represent different points in a *memory–flexibility tradeoff*: HyDia-GPU-DG is algorithmically simpler but requires ~ 27 GB of peak GPU memory (dominated by rotation keys and runtime intermediates), while BSGS-GPU-PRS requires only ~ 9 GB

for 8,192 vectors by using on-demand BSGS rotations and a reduced rotation-key set, at the cost of a slightly more complex online pipeline. Notably, BSGS-GPU-PRS was preferred over the BSGS-Diagonal algorithm (Section 4), since BSGS-Diagonal requires all ℓ query rotations to be kept in GPU memory, while BSGS-GPU-PRS only keeps n_1 of them, leading to an n_2 -factor memory saving. Other approaches prioritizing speed over memory are possible and will be explored in the future. A further variant, BSGS-GPU-PRE (described in Section 5.3.3), shifts the diagonal pre-rotation to the enroller, eliminating negative rotation keys entirely.

Both GPU variants share a common three-layer architecture. At the bottom, FIDESlib [12] provides CUDA-accelerated CKKS primitives (`mult`, `add`, `rotate`, `rescale`, `square`, `copy`, `addScalar`, `multScalar`, `dropToLevel`) that map one-to-one onto their OpenFHE CPU counterparts. A middleware layer orchestrates diagonal caching, rotation caching, Chebyshev evaluation, and aggregation using these primitives. At the top, variant-specific sender modules implement the full query pipelines. Data transfer between host and device is a two-step process: uploading converts an OpenFHE ciphertext to FIDESlib’s intermediate “raw” format and then creates a GPU-resident ciphertext, while downloading reverses the process. Because this conversion is non-trivial, the system follows an *upload-once, compute-many, download-once* pattern: the entire query processing pipeline – similarity computation, Chebyshev comparison, and result aggregation – executes on the GPU, with at most n_1 ciphertexts uploaded per query (a single query ciphertext for HyDia-GPU-DG; n_1 baby-step ciphertexts for BSGS-GPU-PRS—computing these rotations directly on the GPU would require uploading n_1-1 baby-step rotation keys (~ 814 MB for $n_1 = 23$), negating BSGS-GPU-PRS’s memory advantage) and one (membership) or G (identification) ciphertexts downloaded as the result. An additional benefit of this GPU-resident design is a reduction in *host* RAM usage: by offloading cached diagonals and intermediate ciphertexts to GPU memory, the GPU variants consume 24–53% less host RAM than their CPU counterparts. We first describe four common infrastructure components and then detail the per-variant specializations.

5.1. Common GPU infrastructure

5.1.1. Offline caching of encrypted database and keys

A key design decision common to both GPU variants is that the entire encrypted database and all required rotation keys are uploaded to GPU memory once dur-

ing system setup as a one-time cost and remain resident across queries. Concretely, during the offline phase:

1. All encrypted diagonal ciphertexts $\{\text{diag}_i(\mathbf{M}_k)\}$ are deserialized from disk in parallel using OpenMP thread-level parallelism and uploaded to GPU memory.
2. All rotation keys required by the specific variant are pre-initialized on the GPU during setup rather than on the first query, significantly reducing first-query latency.
3. The CUDA stream pool is initialized (see below Section 5.1.2).

The GPU memory requirement is dominated by the diagonals ($G \times \ell$ ciphertexts at ~ 5 MB each for our parameter set) and the rotation keys (~ 37 MB each, including working buffers for key-switching decomposition). Before loading, each variant estimates the total memory requirement (diagonals plus rotation keys) and compares it against a lion’s share of total GPU memory; if the budget is exceeded, the system gracefully falls back to CPU-only computation. Within the remaining free memory, the stream pool (Section 5.1.2) reserves some memory for concurrent per-matrix intermediates, ensuring that runtime allocations do not cause out-of-memory failures.

5.1.2. Multi-stream matrix parallelism

When the database contains K vectors packed into $G = \lceil K/\text{numSlots} \rceil$ matrix groups, each matrix can be processed independently during the online phase. Both GPU variants exploit this by allocating a pool of S CUDA streams and dispatching matrices in waves of up to S concurrent tasks. The pool size is determined at initialization by

$$S = \min\left(\lfloor \frac{\text{SMs}}{4} \rfloor, \lfloor \frac{0.2 \cdot F}{40 \cdot C} \rfloor, 32\right), \quad S \geq 2, \quad (6)$$

where SMs is the GPU’s streaming multiprocessor count, F is free GPU memory, and C is the estimated ciphertext size. The first term ensures that each stream has enough SMs for efficient kernel execution; the second prevents out-of-memory failures from concurrent intermediates (each in-flight matrix requires ~ 40 ciphertext-sized temporary buffers for BSGS products and Chebyshev intermediates). All streams use the `cudaStreamNonBlocking` flag, enabling independent scheduling without implicit synchronization with the default stream. Equation 6 is a practical sizing heuristic derived from profiling and memory traces on our target

GPUs. The divisor 4 in $\lfloor \text{SMs}/4 \rfloor$ allocates about four SMs per active stream, which maintained good occupancy without excessive kernel contention in our workloads. The factor 40 in the memory term comes from the worst-case number of live temporary ciphertext buffers per in-flight matrix in our implementation (similarity + Chebyshev pipeline). The hard cap 32 avoids oversubscription: beyond 32 streams, we observed negligible throughput gains but higher scheduling overhead and memory pressure. Note that the formula adapts dynamically to each GPU’s SM count and available memory; for example, on an NVIDIA H200 (132 SMs), the SM-based term yields $\lfloor 132/4 \rfloor = 33$, which is clipped to the empirically validated cap of 32.

5.1.3. GPU-resident rotation caching

HyDia-GPU-DG computes and caches all $\ell-1$ rotated query ciphertexts directly on the GPU, using FIDESlib’s native copy and rotate operations with zero host–device transfer overhead.

BSGS-GPU-PRS instead computes its n_1-1 baby-step rotations on the CPU (via OpenFHE’s `EvalRotate`) and uploads the resulting ciphertexts to GPU memory. This design avoids uploading n_1-1 baby-step rotation keys to the GPU (~ 814 MB for $n_1 = 23$), preserving VRAM for database diagonals—consistent with BSGS-GPU-PRS’s memory-efficiency goal. The total latency is comparable: CPU rotations plus ciphertext upload matches the GPU-rotation alternative, while consuming $8\times$ less peak GPU memory for the baby-step phase (115 MB vs. 929 MB).

In both variants, the cached baby-step ciphertexts are reused across all G matrix groups without further host–device transfers.

5.1.4. GPU-native Chebyshev comparison

After offloading the similarity computation to the GPU, the Chebyshev comparison remains the only remaining CPU-bound step. Although GPU Chebyshev evaluation is fast (~ 20 ms per matrix group for the full Paterson–Stockmeyer evaluation of a degree-13 Chebyshev polynomial, including power-tree construction, chunk assembly, and Horner combination [55]), a hybrid approach that offloads only the Chebyshev step to the GPU while keeping similarity on the CPU yields minimal improvement, because the per-matrix similarity—not the comparison—dominates overall query time. We therefore implement the entire pipeline, including the Chebyshev evaluation, natively on the GPU to eliminate all host–device round-trips. This differs from the optimized CPU HyDia comparison path (the “f4” variant used in [14, Section 5.4]):

on CPU, that specialization is beneficial because it is tightly coupled to CPU-side execution and memory locality, whereas on GPU it would introduce additional control-flow complexity with limited gain. For GPU execution, a single Paterson–Stockmeyer-based path for both variants gives better end-to-end behavior by keeping all intermediates device-resident and mapping naturally to batched ciphertext kernels.

Both GPU variants share the same encrypted comparison implementation, which evaluates a Chebyshev polynomial approximation to the sign function entirely on the GPU. Beyond its computational role, the encrypted comparison serves a security purpose: by returning only a binary match/non-match indicator rather than the raw encrypted similarity score, it prevents the querier from learning exact distances to database entries—information that could otherwise enable database-reconstruction attacks in which an adversary triangulates individual embeddings from repeated queries. Given an encrypted similarity score ct_s and a threshold δ , we compute

$$f(x) = \frac{1}{2}(\text{sign}(x - \delta) + 1) \approx \begin{cases} 1 & x \geq \delta, \\ 0 & x < \delta, \end{cases} \quad (7)$$

slot-wise on the ciphertext. The sign function is approximated by a degree- n Chebyshev series $\text{sign}_\delta(x) = \sum_{i=0}^n c_i T_i(x)$, where $T_i(x)$ denotes the i -th Chebyshev polynomial of the first kind, defined by the recurrence $T_0(x) = 1$, $T_1(x) = x$, and $T_{k+1}(x) = 2xT_k(x) - T_{k-1}(x)$. The coefficients $\{c_i\}$ are computed offline via Discrete Cosine Transform (DCT)-based interpolation. The polynomial degree is determined by the comparison depth budget κ via a Paterson–Stockmeyer-aware lookup table (e.g., $\kappa = 7 \mapsto 5$, $\kappa = 8 \mapsto 13$, $\kappa = 9 \mapsto 27$, $\kappa = 10 \mapsto 59$); both GPU variants use $\kappa = 8$, yielding $n = 13$, for efficiency purposes.

Paterson–Stockmeyer evaluation. Naive Horner evaluation of a degree- n polynomial on encrypted data requires $O(n)$ multiplicative depth. We instead use the Paterson–Stockmeyer (PS) algorithm [55], which restructures the evaluation into a baby-step/giant-step decomposition using only $O(\sqrt{n})$ depth. To avoid confusion with the BSGS parameters n_1 and n_2 used elsewhere (Sections 3.4 and 5.3), we denote the PS baby-step degree by d_1 and the PS giant-step count by d_2 . The PS algorithm selects d_1 and d_2 minimizing $d_1 + d_2$ subject to $d_1 \cdot 2^{d_2-1} \geq n$. For $n = 13$, the decomposition uses $d_1 = 2$, $d_2 = 4$. The evaluation proceeds in three stages (detailed in Algorithm 2): (1) baby-step Chebyshev powers T_1, \dots, T_{d_1} via a binary doubling

Algorithm 2 GPU Chebyshev sign approximation (Paterson–Stockmeyer)

Require: Encrypted similarity ciphertext ct_s on GPU, Chebyshev coefficients $\{c_i\}_{i=0}^n$ (precomputed on CPU), baby-step degree d_1 , giant-step count d_2 , threshold δ
Ensure: Encrypted comparison ciphertext on GPU (slot values ≈ 1 for match, ≈ 0 otherwise)

```

    ▶ Step 1: Baby-step Chebyshev powers via binary tree
1:  $T[1] \leftarrow ct_s$  ▶  $T_1(x) = x$ 
2: for  $i = 2$  to  $d_1$  do
3:   if  $i$  is a power of 2 then
4:      $T[i] \leftarrow 2 \cdot T[[i/2]]^2 - 1$  ▶ doubling:  $T_{2j}(x) = 2T_j(x)^2 - 1$ 
5:   else
6:      $T[i] \leftarrow 2 \cdot T[[i/2]] \cdot T[[i/2]] - T[1]$  ▶  $i$  odd
7:    $T_{a+b} = 2T_a T_b - T_{|a-b|}$  ▶ product:
8:   end if
9:    $\text{Rescale}_{\text{GPU}}(T[i])$ 
10:   $\text{MatchLevel}_{\text{GPU}}(T[1], T[i])$  ▶ drop  $T[1]$  to match if needed
10: end for

    ▶ Step 2: Giant-step powers by repeated doubling
11:  $T_2[0] \leftarrow T[d_1]$  ▶  $T_{d_1}(x)$ 
12: for  $j = 1$  to  $d_2 - 1$  do
13:    $T_2[j] \leftarrow 2 \cdot T_2[j-1]^2 - 1$  ▶  $T_{d_1 \cdot 2^j}(x)$ 
14:    $\text{Rescale}_{\text{GPU}}(T_2[j])$ 
15: end for

    ▶ Step 3: Chunk polynomials and Horner combination
16: for  $j = 0$  to  $2^{d_2-1} - 1$  do ▶ compute chunk polynomials  $Q_j$ 
17:    $Q[j] \leftarrow c_{j \cdot d_1}$  ▶ constant term (scalar)
18:   for  $i = 1$  to  $d_1 - 1$  do
19:     if  $c_{j \cdot d_1 + i} \neq 0$  then
20:        $Q[j] \leftarrow Q[j] + c_{j \cdot d_1 + i} \cdot T[i]$  ▶ scalar–ciphertext
21:     end if
22:   end for
23: end for

24:  $\text{result} \leftarrow Q[2^{d_2-1} - 1]$  ▶ start from highest chunk
25: for  $j = d_2 - 1$  down to 1 do ▶ Horner-like combination via giant steps
26:    $\text{MatchLevel}_{\text{GPU}}(\text{result}, T_2[0])$ 
27:    $\text{result} \leftarrow \text{result} \cdot T_2[0]$ 
28:    $\text{Rescale}_{\text{GPU}}(\text{result})$ 
29:    $\text{MatchLevel}_{\text{GPU}}(\text{result}, Q[j-1])$ 
30:    $\text{result} \leftarrow \text{result} + Q[j-1]$ 
31: end for

32:  $\text{result} \leftarrow \text{result} + 1.0$  ▶ shift from  $[-1, 1]$  to  $[0, 2]$ 
33: return result

```

tree; (2) giant-step powers $T_{d_1 \cdot 2^j}$ by repeated squaring; (3) chunk polynomials Q_j assembled from the Chebyshev coefficients and combined via Horner’s rule using the giant-step powers.

Depth and level management. The implementation operates in CKKS FIXEDMANUAL rescaling mode, requiring explicit ciphertext level management. Two invariants are maintained: (i) before every ciphertext–

ciphertext multiplication, the operands’ noise level must be 1 (a pending rescale is applied first); (ii) before every addition, both operands must share the same RNS level (achieved via `MatchLevel`, which mod-switches the higher-level operand down). Scalar–ciphertext multiplications do not consume a multiplicative level. In particular, FIDESlib’s `square()` operation strictly enforces invariant (i): it produces incorrect results if the input’s noise level exceeds 1, requiring an explicit rescale before every squaring, even in cases where OpenFHE’s CPU implementation would tolerate a pending rescale. The binary-tree construction achieves $O(\log d_1)$ depth for d_1 baby-step Chebyshev polynomials, and the Horner combination adds $O(d_2)$ levels, yielding a total of ~ 7 multiplicative levels for the comparison ($d_1 = 2$, $d_2 = 4$)—significantly fewer than the 13 levels that Naive Horner evaluation would require.

5.2. HyDia on GPU

HyDia-GPU-DG is the GPU port of the original HyDia diagonal method (described in Section 3.5). Although the BSGS optimization reduces the CPU rotation count from ℓ to $O(\sqrt{\ell})$, the naive diagonal method can be seen as a viable GPU candidate for the fact that all ℓ multiplications per matrix are independent and can execute in parallel, and the ℓ query rotations are computed once and reused across all M matrices. Because non-hoisted GPU rotations are faster than non-hoisted CPU rotations, the cost of computing all ℓ rotations on the GPU is smaller than on the CPU. However, the trade-off is GPU memory: storing $\ell - 1$ rotation keys requires ~ 18.7 GB (including key-switching decomposition buffers), and the total peak GPU memory including cached queries, diagonals, and runtime intermediates reaches ~ 27 GB even at $G=1$, which limits the database size on memory-constrained GPUs—a limitation that BSGS-GPU-PRS addresses. We now describe the different steps of the HyDia protocol on GPU.

Offline phase. Deserialized $G \cdot \ell$ standard diagonal ciphertexts and $\ell - 1$ rotation keys are uploaded to GPU memory.

Online phase.

1. **Query rotations:** Compute $\text{rotQ}[i] = \text{Rot}_i(\mathbf{q})$ for $i \in [0, \ell - 1]$ on the GPU using FIDESlib’s native rotation. All ℓ rotated queries are cached in GPU memory.
2. **Similarity:** For each matrix \mathbf{M}_k , compute $\text{sim}_{\mathbf{M}_k} = \sum_{i=0}^{\ell-1} \text{rotQ}[i] \odot \text{diag}[k \cdot \ell + i]$ where $\text{diag}[k\ell +$

$i]$ denotes the GPU-resident ciphertext encoding $\text{diag}_i(\mathbf{M}_k)$ from Equation 1—via element-wise multiplication with lazy/deferred relinearization (accumulate products first, then relinearize once), followed by rescale—all on the GPU.

3. **Chebyshev and aggregation:** Each similarity ciphertext passes through the GPU Chebyshev comparison (Algorithm 2), and the membership aggregation (tree-reduce addition and rotate-and-sum) runs on the GPU as well.

A full-pipeline function processes all matrices in CUDA waves using the stream pool, performing similarity, Chebyshev, and aggregation entirely on the GPU before downloading a single result ciphertext.

5.3. BSGS with pre-rotated diagonals on GPU

BSGS-GPU-PRS is the GPU port of a BSGS variant (building on the textbook BSGS identity of Section 3.4) with pre-rotated diagonals and on-demand giant-step rotations. The primary motivation for a BSGS-based GPU variant is *GPU memory efficiency*: HyDia-GPU-DG requires $\ell - 1 = 511$ rotation keys (~ 18.7 GB), limiting the database size that fits in GPU memory. By reducing the online rotation-key set to a much smaller BSGS subset (giant-step and EvalSum keys only—baby-step keys remain on the CPU), BSGS-GPU-PRS reduces the peak GPU memory footprint from ~ 27 GB to ~ 9 GB for 8,192 vectors, enabling deployment on GPUs with as little as 12 GB of VRAM. BSGS-GPU-PRS also has a significantly faster setup phase, since uploading this reduced key set is much faster than uploading all HyDia rotation keys.

The key algorithmic change of BSGS-GPU-PRS is that the diagonals are pre-rotated during the offline phase, enabling *on-demand* BSGS execution entirely on the GPU. Without pre-rotation, one could still use BSGS to reduce the rotation key count: compute only n_1 baby-step rotations plus G giant-step rotations via hoisted composition, then run the standard diagonal method with all ℓ pre-composed rotations—this is exactly how our CPU variant (Section 4) operates. However, this approach requires storing all ℓ composed rotations in GPU memory before the matrix–vector product begins. On-demand BSGS avoids this by computing each giant-step contribution *during* the matrix–vector product, accumulating n_1 baby-step products and then applying a single giant-step rotation per group. The difficulty is that ciphertext rotation distributes over products— $\text{Rot}_r(A \cdot B) = \text{Rot}_r(A) \cdot \text{Rot}_r(B)$ —so a giant-step rotation of the accumulated baby-step products

would incorrectly rotate the diagonal components as well. Pre-rotating the diagonals during the offline phase absorbs this offset in advance, restoring correctness (see Equation 8 below). We do not apply this pre-rotation on CPU because the CPU pipeline already uses hoisted composition effectively and is not constrained by GPU-resident rotation caches; the extra offline preprocessing is therefore less beneficial there.

5.3.1. Pre-rotated diagonals

During enrollment, for each giant-step index $j \in \{0, \dots, n_2-1\}$ and baby-step index $i \in \{0, \dots, n_1-1\}$, instead of storing the diagonal ciphertext diag_{jn_1+i} (cf. Equation 1) directly, we store

$$\text{diag}'_{jn_1+i} = \text{Rot}_{-jn_1}(\text{diag}_{jn_1+i}). \quad (8)$$

This pre-rotation absorbs exactly the $\text{Rot}_{-jn_1}(\cdot)$ factor that would otherwise be applied to the diagonal term during the online evaluation. Substituting Equation 8 into the standard BSGS identity (Equation 3) and noting that $\text{Rot}_{jn_1} \circ \text{Rot}_{-jn_1}$ is the identity, the on-demand computation $\text{Rot}_{jn_1}(\sum_i \text{Rot}_i(\mathbf{q}) \odot \text{diag}'_{jn_1+i})$ recovers exactly the standard BSGS result.

Operationally, this means the server computes only n_1 baby-step rotations and, for each giant step j , applies one rotation $\text{Rot}_{j \cdot n_1}(\cdot)$ to the accumulated baby-step products.

5.3.2. Online pipeline

We now describe the different steps of our pipeline.

Offline phase. Standard diagonal ciphertexts from disk are loaded and *pre-rotated on the GPU*: for each diagonal index jn_1+i , the rotation $\text{Rot}_{-jn_1}(\text{diag}_{jn_1+i})$ is applied using FIDESlib’s GPU rotation before caching. Negative giant-step rotation keys $(-n_1, -2n_1, \dots)$ are uploaded to the GPU for this pre-rotation and then *freed* to reclaim GPU memory once all diagonals have been cached. Giant-step keys $(n_1, 2n_1, \dots)$ and power-of-two rotation keys (for the membership scenario’s slot-wise RotateAndSum aggregation) are uploaded and remain GPU-resident for the online phase. (The power-of-two keys are not needed for the identification scenario, which downloads per-matrix results without aggregation.) Baby-step rotation keys are *not* uploaded to the GPU; instead, baby-step rotations are computed on the CPU and the resulting ciphertexts are uploaded (see Section 5.1.3).

Online phase.

1. **Baby-step rotations:** Compute n_1 baby-step rotations of the query ciphertext on the CPU and upload the resulting ciphertexts to GPU memory (see Section 5.1.3).
2. **On-demand BSGS:** For each matrix m and each giant step j :
 - Multiply each baby step $\text{Rot}_i(\mathbf{q})$ with the pre-rotated diagonal diag'_{jn_1+i} , accumulate with lazy/deferred relinearization, and rescale.
 - Apply on-demand giant-step rotation $\text{Rot}_{j \cdot n_1}(\text{sum}_j)$, which correctly aligns the baby-step component without affecting the diagonal (since it was pre-rotated).
3. **Chebyshev plus aggregation:** The full-pipeline function processes all matrices in CUDA waves using the stream pool.

Rotation keys. BSGS-GPU-PRS uses a reduced online key set on the GPU—giant-step keys and powers-of-two EvalSum keys (~ 36 keys total)—roughly an order of magnitude fewer than HyDia-GPU-DG’s 516-key set $((\ell-1) + \lceil \log_2(N/\ell) \rceil)$: 511 diagonal rotation keys plus 5 power-of-two EvalSum keys), freeing substantial GPU memory for larger databases. Baby-step rotation keys exist only in the CPU-side OpenFHE context for computing baby-step rotations before upload. In addition, n_2-1 negative giant-step keys are temporarily uploaded to the GPU for offline diagonal pre-rotation and then freed once all diagonals have been cached. Including these temporary offline keys, the total number of rotation keys generated by the client is ~ 75 .

5.3.3. Variant: enroller-side plaintext pre-rotation (BSGS-GPU-PRE)

BSGS-GPU-PRS applies the diagonal pre-rotation of Equation 8 *homomorphically on the GPU* during the offline phase, requiring n_2-1 negative giant-step rotation keys. An alternative variant, BSGS-GPU-PRE, shifts this pre-rotation to the *enroller* by applying it in the plaintext domain *before* encryption. For each diagonal index jn_1+i , the enroller cyclically rotates the plaintext coefficient vector by $-jn_1$ positions and then encrypts the rotated plaintext. Because the rotation is applied before encryption, it is exact and incurs only $O(\ell)$ data movement per diagonal—negligible compared to the CKKS encryption cost ($\sim 8\%$ enrollment overhead at $K=65,536$).

The key advantage of BSGS-GPU-PRE is that it eliminates all negative giant-step rotation keys: the server never performs homomorphic rotation during diagonal

upload, reducing the total client key count from ~ 75 to ~ 53 and lowering peak GPU memory from ~ 9 GB to ~ 7 GB at $K=8,192$ (a $\sim 22\%$ reduction). The offline diagonal upload reduces to a bulk ciphertext transfer without any GPU rotation, yielding a faster setup phase.

The online phase of BSGS-GPU-PRE is *identical* to BSGS-GPU-PRS: the same on-demand BSGS pipeline, Chebyshev comparison, and aggregation execute on the pre-rotated diagonal ciphertexts.

NTT representation tradeoff. Despite eliminating offline homomorphic rotations, BSGS-GPU-PRE exhibits a small overhead in online query time compared to BSGS-GPU-PRS. This is attributed to a FIDESlib implementation detail: in BSGS-GPU-PRS, the homomorphic rotation applied during diagonal upload leaves the ciphertext polynomials in Number Theoretic Transform (NTT) evaluation form, which is the native representation for subsequent multiplications. In BSGS-GPU-PRE, diagonals are uploaded directly from disk in coefficient form, requiring an implicit forward NTT conversion at first use during multiplication. With $\ell = 512$ diagonals per matrix group and each NTT costing $\sim 40\text{--}50\ \mu\text{s}$, the accumulated overhead ($\sim 20\text{--}25$ ms per matrix group) is consistent with the observed slowdown. A warm-up NTT pass after uploading could shift this cost to the offline phase, but would not eliminate it.

Tradeoff summary. BSGS-GPU-PRE trades a modest online overhead (from NTT conversion) and an enrollment-time dependency on n_1 for fewer rotation keys, lower GPU memory, faster offline setup, and simpler key management. It is best suited for deployments where n_1 is fixed and re-enrollment is infrequent. BSGS-GPU-PRS retains full flexibility, since the server can re-derive the pre-rotated diagonals for any n_1 without re-enrolling the database.

5.4. Overall algorithm description

The complete GPU-accelerated query processing algorithm consists of an offline phase (executed once at system setup) and an online phase (executed for each query). The online phase is presented in Algorithm 3 for the membership scenario and Algorithm 4 for the identification scenario. The algorithm is parameterized by the rotation strategy: HyDia-GPU-DG uses $n_1 = \ell$ baby steps and no giant steps; BSGS-GPU-PRS and BSGS-GPU-PRE use $n_1 = \lceil \sqrt{\ell} \rceil$ baby steps and $n_2 = \lceil \ell/n_1 \rceil$ on-demand giant steps with pre-rotated diagonals (the two variants differ only in *where* and *how* the pre-rotation is performed; see Section 5.3.3).

Algorithm 3 GPU query processing — Membership

Require: Encrypted query \mathbf{q} , diagonal ciphertexts $\{\text{diag}[\mathbf{M}_\ell]\}$ cached on GPU (pre-rotated for BSGS-GPU-PRS/BSGS-GPU-PRE), rotation parameter n_1 , comparison threshold δ , Chebyshev depth κ , stream pool size S , number of matrices G

Ensure: Encrypted membership result (single ciphertext)

```

1: Upload  $\mathbf{q}$  to GPU
2: for  $i = 0$  to  $n_1 - 1$  do
3:    $\text{baby}[i] \leftarrow \text{Rot}_t(\mathbf{q})$   $\triangleright$  on GPU for HyDia-GPU-DG ( $n_1 = \ell$ ); on CPU
   then uploaded for BSGS-GPU-PRS ( $n_1 = \lceil \sqrt{\ell} \rceil$ )
4: end for

 $\triangleright$  Step 2: Per-matrix similarity + Chebyshev (multi-stream on GPU)
5:  $n_2 \leftarrow \lceil \ell/n_1 \rceil$   $\triangleright n_2 = 1$  for HyDia-GPU-DG;  $n_2 = 23$  for BSGS-GPU-PRS
6: for each wave  $w = 0, S, 2S, \dots$  up to  $G$  do
7:   for  $m = w$  to  $\min(w+S, G)-1$  in parallel (stream  $m \bmod S$ ) do
8:      $\text{acc}_m \leftarrow \mathbf{0}$ 
9:     for  $j = 0$  to  $n_2 - 1$  do
10:       $\text{sum}_j \leftarrow \sum_{i=0}^{\min(n_1, \ell-jn_1)-1} \text{baby}[i] \odot \text{diag}[m \cdot \ell + jn_1 + i]$ 
11:       $\text{Rescale}_{\text{GPU}}(\text{sum}_j)$ 
12:      if  $j > 0$  and  $n_2 > 1$  then
13:         $\text{sum}_j \leftarrow \text{Rot}_{\text{GPU}}(\text{sum}_j, j \cdot n_1)$   $\triangleright$  on-demand giant-step
        rotation (BSGS-GPU-PRS only)
14:      end if
15:       $\text{acc}_m \leftarrow \text{acc}_m + \text{sum}_j$ 
16:    end for
17:     $\text{cheb}_m \leftarrow \text{ChebyshevCompare}_{\text{GPU}}(\text{acc}_m, \delta, \kappa)$   $\triangleright$  Algorithm 2
18:  end for
19:  SynchronizeStreams( $w, \dots, w+S-1$ )
20: end for

 $\triangleright$  Step 3: Aggregation (on GPU)
21:  $\text{result} \leftarrow \sum_{m=0}^{G-1} \text{cheb}_m$   $\triangleright$  tree-reduce addition on GPU
22:  $\text{result} \leftarrow \text{RotateAndSum}_{\text{GPU}}(\text{result}, N)$   $\triangleright$  slot-wise aggregation

 $\triangleright$  Step 4: Download
23: Download result from GPU to CPU

24: return result  $\triangleright$  slot 0 encodes the total match count
```

Algorithm 4 GPU query processing — Identification

Require: Same as Algorithm 3

Ensure: Vector of G encrypted comparison ciphertexts

```

 $\triangleright$  Steps 1–2: identical to Algorithm 3, yielding  $\{\text{cheb}_m\}_{m=0}^{G-1}$  on GPU

 $\triangleright$  Step 3: Bulk download
1: for  $m = 0$  to  $G - 1$  do
2:   Download  $\text{cheb}_m$  from GPU to CPU
3: end for
4: return  $\{\text{cheb}_0, \text{cheb}_1, \dots, \text{cheb}_{G-1}\}$   $\triangleright$  non-zero slots identify matching
   indices
```

5.5. Complexity analysis

Table 2 summarizes the per-query costs of both GPU variants alongside the CPU baseline. In this table, the per-query upload count refers to uploading the query ciphertext \mathbf{q} .

Transfer overhead. Per-query host–device transfer is dominated by the baby-step ciphertext uploads: 1 ciphertext (~ 5 MB) for HyDia-GPU-DG versus n_1 ciphertexts (~ 115 MB) for BSGS-GPU-PRS/BSGS-GPU-PRE—in both cases orders of magnitude less than uploading all ℓ rotations (~ 2.5 GB). Detailed transfer cost measurements are reported in Section 6.4.

Rotation key tradeoff. BSGS-GPU-PRS requires $\sim 10\times$ fewer online rotation keys on the GPU than HyDia-GPU-DG, freeing GPU memory for larger databases. The trade-off is that BSGS-GPU-PRS requires n_2-1 on-demand giant-step rotations per matrix, whereas HyDia-GPU-DG performs no giant-step rotations but pre-computes all $\ell-1$ baby-step rotations.

Pre-rotation tradeoff (BSGS-GPU-PRS). BSGS-GPU-PRS trades additional offline computation (pre-rotating all diagonals during GPU caching) for a smaller online rotation count. Quantitatively, pre-rotation reduces the online giant-step work from $n_1 \times (n_2-1)$ rotations per matrix to n_2-1 , which is the key cost reduction for GPU execution.

Setup vs. query tradeoff. HyDia-GPU-DG incurs a substantially higher one-time setup cost because it uploads and initializes the full diagonal-rotation key set, while BSGS-GPU-PRS initializes only the reduced BSGS key subset plus offline pre-rotation keys. The difference in per-query cost arises because HyDia-GPU-DG must compute 511 baby-step rotations per query and then sequentially accumulate 512 diagonal products per matrix, whereas BSGS-GPU-PRS needs only 22 baby-step rotations and evaluates each matrix via 23 giant-step groups—of which 22 require an on-demand GPU rotation. The BSGS structure maps efficiently to GPU parallelism, replacing 512 sequential products with ~ 23 coarser iterations of n_1 products each, keeping BSGS-GPU-PRS’s per-matrix cost well below HyDia-GPU-DG’s independent of G . BSGS-GPU-PRE shares the same online pipeline as BSGS-GPU-PRS and therefore has the same per-query rotation and multiplication costs; its advantage lies in a faster offline setup (no homomorphic pre-rotation) and fewer rotation keys (~ 53

vs. ~ 75), at the cost of a small NTT-conversion overhead during the online phase (see Section 5.3.3). Concrete setup and query timing comparisons are given in Section 6.4.

6. Experimental results

We run experiments with both CPU and GPU support. For CPU, all of our experiments are ran on the same machine, equipped with an Intel Xeon Platinum 8260 CPU at 2.4 GHz and 250 GB of RAM, running Ubuntu 20.04.6 LTS. We use multi-threading to improve the performance for all variants. Parameters are chosen to satisfy 128-bit security level. We rely on OpenFHE [15] as the FHE library to implement our algorithms (building on the framework already set up by [14]). Our GPU experiments are ran on NVIDIA Quadro RTX 8000, 46,080 MiB VRAM (driver 570.133.20) and we rely on FIDESLib [12] for GPU integration mentioned in the previous section.

6.1. Parameter selection

The vector dimension is chosen to be $\ell = 512$ following standard face feature extractors [14, 50].

Parameter selection for HyDia (original). We initially do not modify the parameters that were chosen in the original submission for [14]. Therefore, the ring dimension is 2^{15} resulting in a batch size of 2^{14} . The multiplicative depth is set to 11 with the comparative depth (for Chebyshev) set to $\kappa = 10$. The scaling factor is set to 45. Other remaining parameters are automatically selected to satisfy a 128-bit security level. In our GPU experiments, we have also tested lowering the comparative depth to $\kappa = 8$, resulting in a total multiplicative depth of 9 (see Figure 4 and Table C.6).

Parameter selection for BSGS-Diagonal. For fair comparison, we run our CPU BSGS-Diagonal with the same CKKS parameters, namely the same ring size (resulting in 2^{14} slots), a scaling factor of 45. For the total multiplicative depth, we run experiments with 11 (as for HyDia) but also lower it to 9 for CPU code. For our GPU experiments, the total multiplicative depth is $8 + 2 + 1 = 11$. For BSGS, we selected the baby-step parameter as $n_1 = 23$ (manually optimized for performance) and the giant-step parameter is thus $n_2 = \lceil 512/23 \rceil = 23$.

Table 2: Per-query operation and transfer costs. $\ell=512$, $n_1=23$, $n_2=23$, $G=\lceil K/\text{numSlots} \rceil$ matrix groups. HyDia-GPU-DG’s 516 keys comprise $\ell-1 = 511$ diagonal rotation keys plus 5 power-of-two EvalSum keys.

Resource	CPU	HyDia-GPU-DG	BSGS-GPU-PRS	BSGS-GPU-PRE
Baby-step rotations	$\ell-1$	$\ell-1$ (GPU)	n_1-1 (CPU)	n_1-1 (CPU)
Giant-step rotations	—	—	$(n_2-1)\cdot G$	$(n_2-1)\cdot G$
Total online rotations	$\ell-1$	$\ell-1$	$(n_1-1)+(n_2-1)\cdot G$	$(n_1-1)+(n_2-1)\cdot G$
Mult. per matrix	ℓ	ℓ	ℓ	ℓ
CPU \rightarrow GPU upload	—	1 ct	n_1 cts	n_1 cts
GPU \rightarrow CPU download	—	$1/G$ cts	$1/G$ cts	$1/G$ cts
Rotation keys (total)	—	516	~ 75	~ 53
Keys on GPU (online)	—	516	36	36
Peak GPU memory ($K=8192$)	—	~ 27 GB	~ 9 GB	~ 7 GB
Pre-rotated diags	No	No	Server (HE)	Enroller (PT)
Negative rot. keys	No	No	Yes (freed)	No

Datasets. Our experiments use synthetic datasets. Each synthetic dataset is generated by a Python script that takes as input the database size K , the number of matching vectors K_m , and an optional random seed for reproducibility. Every vector has dimension $\ell = 512$. A query vector \mathbf{q} is drawn uniformly at random with integer components in $[-99, 99]$. The K_m matching database vectors are created by adding small per-component noise (uniform in $[-2, 2]$) to \mathbf{q} , ensuring reasonable cosine similarity with the query; their positions in the database are chosen uniformly at random as well. The remaining $K - K_m$ non-matching vectors are drawn independently and uniformly in $[-99, 99]^\ell$. In our benchmarks, we use varying K_m matching vectors, and database sizes range from 2^{10} to 2^{20} .

6.2. Benchmarking methodology

Each configuration (approach \times database size \times comparison depth) is executed for $t = 11$ independent trials. All experiments use multi-threaded execution via OpenMP with the thread count fixed at 40. This value was empirically determined to be optimal on our 24-core / 48-thread Xeon Platinum 8260: using all 48 hardware threads incurs hyperthreading contention on memory-bandwidth-bound HE operations, while 40 threads saturates the memory subsystem without excessive context-switching overhead.

Trial design. All trials within a configuration share the same cryptographic key pair and encrypted database, isolating query-time variability from key-generation and enrollment randomness. Concretely, the key pair and all database ciphertexts are generated once during the first trial and serialized to disk; trials 2 through 11 deserialize the existing material and proceed directly to query evaluation. The plaintext dataset—a

synthetic collection of $\ell = 512$ -dimensional integer vectors with K_m planted matching entries—is likewise generated once per (K, K_m) pair and held constant across all 11 trials.

Measurements. For each trial, an automated benchmark harness launches the system under test as a subprocess and collects four timing measurements: (i) *wall-clock time* (measured by the harness around the entire subprocess), (ii) *enrollment time* (reported by the system at the end of database encryption), (iii) *membership query time* (server-side computation only, excluding client-side encryption, decryption, and network transmission), and (iv) *identification query time* (same exclusion). A background monitoring thread samples three resource metrics at 0.5s intervals: peak resident memory (RSS) of the process, peak disk usage of the serialized key and ciphertext store, and—for GPU approaches—peak GPU VRAM via the NVIDIA Management Library.

Correctness validation. Every trial automatically checks two correctness conditions: (i) the membership result must match the ground truth (positive iff $K_m > 0$), and (ii) the identification result must return exactly the set of planted matching indices. A trial is marked `PASS` only if both conditions hold and the process exits successfully; otherwise, it is marked `FAIL` and excluded from timing aggregation.

Warm-up and aggregation. The first trial in each configuration includes one-time costs that are not representative of steady-state query latency: key generation and serialization, encrypted-database construction, first-touch memory page faults, and—for GPU approaches—lazy CUDA context and memory pool initialization. To separate these setup costs from the per-query performance, we distinguish *trial 1* from *trials 2–11*. For query-time metrics (membership and identification), we

report the mean \pm standard deviation over the last $N = t-1 = 10$ trials (i.e., trials 2–11), denoted *last-N* throughout. We use the population standard deviation, since the N measurements constitute the entire set of observations rather than a sample from a larger population. Enrollment time and peak disk usage are inherently one-time costs and are therefore reported from trial 1 only. Peak RAM is reported as the mean \pm std over the last- N trials to reflect steady-state memory consumption. The wall-clock “overall” time reported in summary tables is computed as enroll(trial 1) + mean(wall time, last N), reflecting a realistic end-to-end cost for a first deployment followed by a representative query. Unless otherwise stated, all timing values in our tables and figures refer to the *last-N* mean \pm std.

Remark 2. Note that membership and server timings are not end-to-end in our benchmarks. The network transmission can be simulated following Table 6 of the original HyDia work [14], where for network bandwidths of 1 Gbps and above the impact seems to be minimal during a querying phase.

6.3. Performance and memory tradeoffs with BSGS (CPU)

Client-side: rotation keys required for HyDia and BSGS-Diagonal. Recall that $\ell = 512$ and $\text{numSlots} = 16384$. For HyDia, the number of required rotation keys is $\ell - 1 = 511$. Note that this number is independent from the database size and only depends on the ring dimension and the embedding dimension.

For BSGS-Diagonal, the number of rotation keys also depends on the BSGS parameter n_1 and the key count is also independent from the database size. Again, let $\ell = 512$, $\text{numSlots} = 16384$, and $n_1 = 23$. The rotation indices consist of $S_{\text{baby}} = \{1, \dots, 22\}$ and $S_{\text{giant}} = \{23, 46, \dots, 506\}$ which results in a total number of $22 + 22 = 44$ rotation keys.

Hence, for any database size, HyDia requires 511 rotation keys while our BSGS-Diagonal only requires 44 rotation keys, i.e., 91% fewer rotation keys. As a rotation key occupies about 30 MB in RAM based on our experiments, the memory saving in rotation keys is about 14 GB memory, a significant relief for the client.

Overall performance and peak RAM. To evaluate our BSGS-Diagonal algorithm against the diagonal method used by HyDia, we run both algorithms for membership and index scenarios and compare the execution time (in seconds), the peak RAM (in GB) and the peak disk usage (in GB) for datasets of size 2^{10} to 2^{20} . Figure 3 illustrates our results. In terms of performance, our new

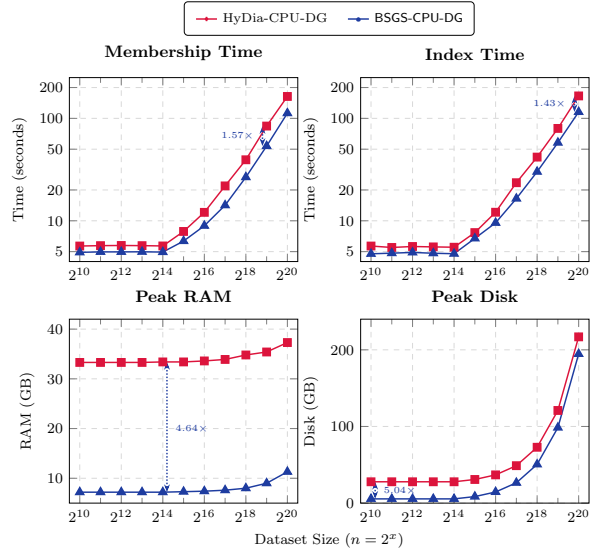


Figure 3: Comparing the original HyDia and our BSGS-Diagonal optimization on CPU for membership and index scenarios execution time and peak RAM and Disk usage for databases from 2^{10} - 2^{20} . Numbers are reported for total multiplicative depth 11.

variant slightly improves on HyDia with up to a 1.57 \times and 1.43 \times speed-up for the database of size 2^{19} for the membership scenario and for the database of size 2^{20} for the identification scenario respectively. The biggest advantage of our method is in the reduced memory consumption and we get up to 4.6 \times reduction of peak RAM and 5 \times reduction in disk usage (for databases of size 2^{10}) and similar reductions for all our databases up to size 2^{18} . Notably, with our method, the peak RAM never exceeds 8 GB for databases up to 2^{18} (as opposed to the 33 GB for HyDia), making our algorithm much more suited to deployment on constrained edge devices. We report our exact experimental results in Table C.5 in Appendix C.

6.4. GPU acceleration

Rotation keys and GPU memory. HyDia-GPU uses 511 rotation keys (same as HyDia on CPU) at ~ 37 MB each (~ 18.7 GB for keys alone). With cached diagonals and intermediate buffers, HyDia-GPU-DG on GPU requires ~ 24 GB of GPU memory for a database of 8,192 vectors – feasible on high-end GPUs (e.g., NVIDIA RTX 8000 with 48 GB or H200 with 141 GB).

Transfer overhead. HyDia-GPU-DG uploads a single query ciphertext (~ 5 MB) per query and computes all $\ell-1$ baby-step rotations directly on the GPU. BSGS-GPU-PRS and BSGS-GPU-PRE instead upload $n_1 =$

23 baby-step ciphertexts (~ 115 MB) per query, pre-computed on the CPU. In both cases, this is far less than the $\ell = 512$ ciphertexts (~ 2.5 GB) that would be required if all query rotations were computed on the CPU and uploaded to the GPU.

Setup vs. query cost. BSGS-GPU-PRS is faster per query than HyDia-GPU-DG: at $K=1,024$, BSGS-GPU-PRS achieves 0.25 s membership latency versus 0.63 s for HyDia-GPU-DG (2.5 \times faster); at $K=65,536$, HyDia-GPU-DG exceeds GPU memory entirely, while BSGS-GPU-PRS completes in ~ 3.0 s. HyDia-GPU-DG also incurs a substantially higher one-time setup cost: approximately 39 s wall time versus ~ 9.5 s for BSGS-GPU-PRS and ~ 8.5 s for BSGS-GPU-PRE at $K=1,024$, due to the overhead of uploading and initializing all 516 rotation keys.

Performance improvement. As explained in Section 5, both HyDia’s original code and our new algorithm were adapted to GPU and Figure 4 illustrates the improvements we obtain by moving from CPU to GPU. More precisely, we improved HyDia-GPU-DG by up to 6.8 \times and 9.7 \times for the membership and index scenarios, respectively, and BSGS-GPU-PRS by up to 17 \times in both scenarios. Note that the improvement for BSGS-GPU-PRS is more significant than for HyDia-GPU-DG (approximately 2 \times greater) because BSGS requires far fewer rotation keys (44 vs. 511), reducing the key material that must reside in GPU memory and freeing more resources for parallel computation. However, these peak speedups are observed at smaller databases ($K \leq 2^{14}$); at $K=2^{15}$, HyDia-GPU-DG’s membership speedup drops to 3.4 \times and BSGS-GPU-PRS’s to 7.7 \times , and at $K=2^{16}$ BSGS-GPU-PRS’s speedup decreases further to 3.2 \times , as larger databases increase GPU memory pressure and reduce the available parallelism. This GPU-based improvement enables sub-second performance for both HyDia-GPU-DG and BSGS-GPU-PRS on databases up to 2^{14} , and sub-second performance for BSGS-GPU-PRS alone up to 2^{15} . In terms of peak RAM usage, BSGS-GPU-PRS reduces memory consumption by up to 8.2 \times compared to the HyDia-CPU baseline (BSGS-GPU-PRE further reduces it to 11.0 \times), whereas HyDia-GPU-DG yields a modest 1.17 \times reduction. For peak disk usage, BSGS-GPU-PRE achieves up to 5.14 \times less disk compared to HyDia-CPU (and BSGS-GPU-PRS up to 4.32 \times), whereas HyDia-GPU-DG actually increases disk usage by $\sim 12\%$ due to additional serialized key material from the GPU library. Using GPU, we were only able to run HyDia-GPU-DG up to databases of size 2^{15} and BSGS-GPU-PRS up to 2^{16} before running

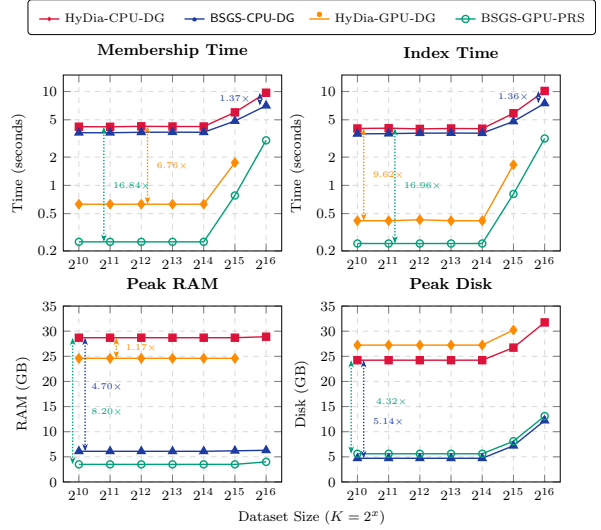


Figure 4: Comparing the original HyDia and our BSGS-Diagonal optimization on CPU and GPU for membership and index scenarios execution time and peak RAM and Disk usage for databases from 2^{10} – 2^{16} (means over 11 trials). The comparison depth considered in these experiments is $\kappa = 8$. GPU experiments use an NVIDIA Quadro RTX 8000.

into out-of-GPU-memory errors due to the large number of rotation keys and ciphertext intermediates exceeding the available 48 GB of VRAM on the RTX 8000. The full benchmark results comparing CPU and GPU performances for the original HyDia and the BSGS variant are presented in Appendix C.2, Table C.6.

7. Conclusion

In this work, we improve the practicality of FHE for encrypted facial matching search in realistic client-server settings where both database and client queries are encrypted. Building on HyDia, we introduced BSGS-Diagonal, a more memory-efficient similarity computation strategy, that reduces the number of required rotation keys while also improving performance. Experimentally on multi-threaded CPUs, it lowers the rotation-key set by 91%, reduces client memory by approximately 14 GB, decreases peak RAM by up to about 4.5 \times , and improves runtime by up to 1.57 \times in membership verification and 1.43 \times in identification.

We also show that significant speed gains can be achieved through a GPU-resident execution pipeline while advancing a fully open-source encrypted database search solution, instantiated here through facial matching. By integrating OpenFHE with FIDESlib and adding GPU-native support for encrypted similarity

evaluation, including a Chebyshev evaluator and optimized similarity computation kernels, we minimize host-device transfers and improve parallel execution. Our GPU implementations achieve up to $9\times$ speedup for HyDia and up to $17\times$ for BSGS-Diagonal, enabling sub-second encrypted face recognition for databases with up to 2^{15} entries while also reducing host memory usage. In particular, our FIDESlib-based design supports full similarity computation inside a GPU kernel, which, to the best of our knowledge, is not currently available in other open-source implementations.

Appendix A. Operation count for the diagonal method vs textbook BSGS

Dimension	Diagonal	BSGS
Multiplications	ℓ	ℓ
Additions	$\ell - 1$	$\ell - 1$
Rotations	$\ell - 1$	$(n_1 - 1) + (n_2 - 1)$
Rotation keys	$\ell - 1$	$(n_1 - 1) + (n_2 - 1)$
Relinearization keys	ℓ	ℓ
Asymptotic rotations	$\Theta(\ell)$	$\Theta(n_1 + n_2) = \Theta(\sqrt{\ell})$
Overall asymptotic cost	$\Theta(\ell)$	$\Theta(\ell)$
Memory for keys (rot + relin)	$\Theta(\ell)$	$\Theta(n_1 + n_2) = \Theta(\sqrt{\ell})$

Table A.3: Asymptotic operation count and memory usage for diagonal encoding vs BSGS. We assume $n_2 = \lceil \ell/n_1 \rceil$.

DB size	G	Total # of Rotations		Memory (# of Rotated CTs)	
		Textbook BSGS	BSGS-Diagonal	Textbook BSGS	BSGS-Diagonal
2^{14}	1	44	511	23	512
2^{16}	4	110	511	23	512
2^{18}	16	374	511	23	512
2^{19}	32	726	511	23	512
2^{20}	64	1430	511	23	512

Table A.4: Comparison of rotations performed and memory usage (number of rotated query ciphertexts simultaneously stored) between single-hoisted textbook BSGS and BSGS-Diagonal for varying database sizes and $n_1 = n_2 = 23$.

Appendix B. HyDia [14] pseudo-codes

Algorithm 5 Enroller (HyDia original):

Require: Database $\mathcal{D} = \{x_i \in \mathbb{R}^{\ell}_{i=1}^K, \text{public key pk, crypto context cc}$

```

1: Normalize database (plaintext):
2: for  $i = 1$  to numVectors do
3:    $x_i \leftarrow \text{Normalize}(x_i, \ell)$ 
4: end for

5: Build  $\ell \times \ell$  squares and extract diagonals (plaintext):
6:  $\{S^{(g)}\} \leftarrow \text{SplitIntoSquareMatrices}(\mathcal{D}, \ell)$   $\triangleright S^{(g)} \in \mathbb{R}^{\ell \times \ell}$ 
7: for each group  $g$  do
8:    $\text{Diags}^{(g)} \leftarrow \text{Diagonals}(S^{(g)})$   $\triangleright$  list of  $\ell$  diagonals, each length  $\ell$ 
9: end for

10: Concatenate diagonals into SIMD-sized rows:
11:  $\{\text{row}_i\} \leftarrow \text{ConcatenateRows}(\{\text{Diags}^{(g)}\})$   $\triangleright$  packs diagonals linearly into plaintext rows

12: Parallel encryption and async I/O:
13: for  $i = 0$  to  $\lceil \text{row}_i \rceil - 1$  do  $\triangleright$  loop is parallelized in implementation
14:    $ct \leftarrow \text{Encrypt}(\text{pk}, \text{row}_i)$ 
15:    $\text{path} \leftarrow \text{"serial/db\_diagonal/index"} + i + \text{"bin"}$ 
16:    $\text{WriteBinaryAsync}(ct, \text{path})$ 
17: end for

```

Appendix C. Full Benchmark Results

We present our detailed performance results for both CPU with BSGS-Diagonal and aggregation techniques

Algorithm 6 COMPUTESIMILARITY

Require: Encrypted query \mathbf{q} , vector dimension ℓ , number of database vectors K , batch size numSlots , cyclotomic order Ω .

```
1:  $G \leftarrow \left\lceil \frac{K}{\text{numSlots}} \right\rceil$   $\triangleright$  number of packed matrices / groups
2:  $\text{similarityCipher} \leftarrow []$ 
3: Precompute for fast hoisted rotations of the query ciphertext
4:  $\text{rotatedQueryCipher} \leftarrow []$ 
5:  $\text{rotatedQueryCipher}[0] \leftarrow \mathbf{q}[0]$ 
6:  $\text{queryPrecomp} \leftarrow \text{EVALFASTROTATIONPRECOMPUTE}(\mathbf{q}[0])$ 

7: for  $1 \leq i \leq \ell - 1$  do  $\triangleright$  can be parallelized
8:    $\text{rotatedQueryCipher}[i] \leftarrow$ 
    $\text{EVALFASTROTATION}(\mathbf{q}[0], i, \Omega, \text{queryPrecomp})$   $\triangleright$  rotate packed query by  $i$ 
   slots
9: end for

10: for  $0 \leq m \leq G - 1$  do
11:    $\text{similarityCipher}[m] \leftarrow$ 
    $\text{COMPUTESIMILARITYMATRIX}(\text{rotatedQueryCipher}, m)$   $\triangleright$  compute
   similarity scores for DB block  $m$  (packed in  $\text{numSlots}$  slots)
12: end for

13: return  $\text{similarityCipher}$ 
```

Algorithm 7 Membership Scenario

Require: Encrypted query \mathbf{q} , threshold τ , comparator depth κ , batch size numSlots .

```
1:  $\text{scoreCipher} \leftarrow \text{COMPUTESIMILARITY}(\mathbf{q})$   $\triangleright$  vector of group ciphertexts,
   each packing scores in  $\text{numSlots}$  slots
2: for  $0 \leq g \leq |\text{scoreCipher}|-1$  do
3:    $\text{scoreCipher}[g] \leftarrow \text{CHEBYSHEVCOMPARE}(\text{scoreCipher}[g], \tau, \kappa)$   $\triangleright$ 
    $\approx 1$  if  $\text{score} \geq \tau$ , else  $\approx 0$ 
4: end for
5:  $\text{membershipCipher} \leftarrow \text{EVALADDMANYINPLACE}(\text{scoreCipher})$   $\triangleright$  sum all
   group ciphertexts into a single ciphertext
6:  $\text{membershipCipher} \leftarrow \text{EVALSUM}(\text{membershipCipher}, \text{numSlots})$   $\triangleright$  sum
   all  $\text{numSlots}$  slots into slot 0
7: return  $\text{membershipCipher}$   $\triangleright$  slot 0 encodes the total count of matches
   across all groups/slots
```

Algorithm 8 Index Scenario

Require: Encrypted query \mathbf{q} , threshold τ , comparator depth κ .

```
1:  $\text{scoreCipher} \leftarrow \text{COMPUTESIMILARITY}(\mathbf{q})$   $\triangleright$  vector of group ciphertexts,
   each packing scores in  $\text{numSlots}$  blocks
2: for  $0 \leq g \leq |\text{scoreCipher}|-1$  do
3:    $\text{scoreCipher}[g] \leftarrow \text{CHEBYSHEVCOMPARE}(\text{scoreCipher}[g], \tau, \kappa)$   $\triangleright$ 
    $\approx 1$  if  $\text{score} \geq \tau$ , else  $\approx 0$ 
4: end for

5: return  $\text{scoreCipher}$ 
```

and GPU compared with the original HyDia code. *Reported metrics.* Tables C.5 and C.6 report the following columns for each configuration:

- K and K_m : the number of vectors in the encrypted database (database size) and the number of uniformly at random planted matching vectors relative to the query, respectively.
- **Approach:** the algorithm variant under test. Names follow the convention *Method-Platform-Variant*: HyDia-CPU-DG (diagonal method, CPU), BSGS-CPU-DG (BSGS-Diagonal, CPU), HyDia-GPU-DG (diagonal method, GPU), BSGS-GPU-PRS (BSGS with server-side diagonal pre-rotation, GPU), and BSGS-GPU-PRE (BSGS with enroller-side diagonal pre-rotation, GPU).
- **RTT (s):** overall wall-clock time in seconds, computed as $\text{enroll}(\text{trial } 1) + \text{mean}(\text{wall time}, \text{last-}N)$. This combines the one-time enrollment cost (database encryption and serialization, measured in the first trial) with the average end-to-end process time over the $N = 10$ steady-state trials. The per-trial wall-clock time spans the full execution of the system under test: key deserialization, query encryption, server-side membership and identification computation, and result decryption. Network transmission is not included. Reported as a single value (no \pm).
- **Membership (s):** server-side membership-query computation time in seconds. This measures only the homomorphic computation on the server: encrypted inner-product evaluation via the diagonal (or BSGS-Diagonal) method, Chebyshev sign approximation, and aggregation across database groups. Client-side operations (query encryption, result decryption) and network transfer are excluded. Reported as $\text{mean} \pm \text{std}$ over the last- N trials.
- **Index (s):** server-side identification-query computation time in seconds. This measures the per-vector encrypted similarity evaluation and index extraction on the server. Like the membership metric, client-side operations and network transfer are excluded. Reported as $\text{mean} \pm \text{std}$ over the last- N trials.
- **RAM (GB):** peak resident set size (RSS) of the process in gigabytes, reflecting the maximum physical memory footprint during the trial. Reported as $\text{mean} \pm \text{std}$ over the last- N trials.

- **Disk (GB):** peak on-disk size (in gigabytes) of the serialized cryptographic material—keys, encrypted database diagonals, and any intermediate ciphertexts—measured by summing all files in the serialization directory. The value is deterministic across trials ($\sigma = 0$), as the serialized material is written once during enrollment and remains unchanged in subsequent trials.

Appendix C.1. CPU-only benchmarks with BSGS-Diagonal

Table C.5 reports our CPU-only benchmark results with $\kappa = 10$, *i.e.*, with total multiplicative depth equal to 11 (as in the original HyDia work). We compare HyDia-CPU-DG against BSGS-CPU-DG, where BSGS-CPU-DG corresponds to BSGS-Diagonal.

Appendix C.2. Additional CPU/GPU benchmark table

Table C.6 reports our CPU and GPU benchmark results with $\kappa = 8$, *i.e.*, the total multiplicative depth is equal to 9. For $K = 2^{16}$, HyDia-GPU-DG observed an out-of-GPU-memory issue.

References

- [1] H. Gururaj, B. Soundarya, S. Priya, J. Shreyas, F. Flammini, A comprehensive review of face recognition techniques, trends, and challenges, *IEEE Access* 12 (2024) 107903–107926.
- [2] G. Mai, K. Cao, P. C. Yuen, A. K. Jain, On the reconstruction of face images from deep face templates, *IEEE transactions on pattern analysis and machine intelligence* 41 (2018) 1188–1202.
- [3] X. Dong, Z. Miao, L. Ma, J. Shen, Z. Jin, Z. Guo, A. B. J. Teoh, Reconstruct face from features based on genetic algorithm using gan generator as a distribution constraint, *Computers & Security* 125 (2023) 103026.
- [4] H. O. Shahreza, S. Marcel, Comprehensive vulnerability evaluation of face recognition systems to template inversion attacks via 3d face reconstruction, *IEEE Transactions on Pattern Analysis and Machine Intelligence* 45 (2023) 14248–14265.
- [5] S. Yan, H. Wen, S. Chang, H. Zhu, L. Zhou, Black-box 3d face reconstruction attack on face recognition from a single image, *IEEE Internet of Things Journal* (2025).
- [6] Z. Wang, H. Wang, S. Jin, W. Zhang, J. Hu, Y. Wang, P. Sun, W. Yuan, K. Liu, K. Ren, Privacy-preserving adversarial facial features, in: *Proceedings of the IEEE/CVF Conference on Computer Vision and Pattern Recognition*, 2023, pp. 8212–8221.
- [7] H. Liu, H. Du, J. Chen, J. Wang, K. Zhang, K. Zhang, P. Liu, Patronus: Plug-and-play and near-lossless facial privacy enhancement against reconstruction attacks, *IEEE Transactions on Information Forensics and Security* (2025).
- [8] H. Liu, L. Ding, J. Chen, J. Wang, X. Du, J. Guo, Adversarial face database against deep learning-enabled reconstruction attacks, *ACM Transactions on Intelligent Systems and Technology* 17 (2026) 1–19.
- [9] J. Ji, H. Wang, Y. Huang, J. Wu, X. Xu, S. Ding, S. Zhang, L. Cao, R. Ji, Privacy-preserving face recognition with learnable privacy budgets in frequency domain, in: *European Conference on Computer Vision*, Springer, 2022, pp. 475–491.
- [10] Y. Mi, Y. Huang, J. Ji, H. Liu, X. Xu, S. Ding, S. Zhou, Duetface: Collaborative privacy-preserving face recognition via channel splitting in the frequency domain, in: *Proceedings of the 30th ACM International Conference on Multimedia*, 2022, pp. 6755–6764.
- [11] Y. Gong, X. Chang, J. Mišić, V. B. Mišić, J. Wang, H. Zhu, Practical solutions in fully homomorphic encryption: a survey analyzing existing acceleration methods, *Cybersecurity* 7 (2024) 5.
- [12] C. Agulló-Domingo, Ó. Vera-López, S. Guzelhan, L. Daksha, A. El Jerari, K. Shivdikar, R. Agrawal, D. Kaeli, A. Joshi, J. L. Abellán, Fideslib: A fully-fledged open-source FHE library for efficient CKKS on GPUs, in: *2025 IEEE International Symposium on Performance Analysis of Systems and Software (ISPASS)*, IEEE, 2025, pp. 1–3.
- [13] J. Cheon, A. Kim, M. Kim, Y. Song, Homomorphic encryption for arithmetic of approximate numbers, in: *Advances in cryptology—ASIACRYPT 2017: 23rd international conference on the theory and applications of cryptology and information security*, Hong kong, China, December 3-7, 2017, proceedings, part i 23, Springer, 2017, pp. 409–437.

Table C.5: CPU-only benchmark results with $\kappa = 10$. We compare HyDia-CPU-DG against BSGS-CPU-DG, where BSGS-CPU-DG corresponds to BSGS-CPU-DG. Values are reported as mean \pm std over 11 trials. The parenthetical value in gray is the ratio against HyDia-CPU-DG as the baseline.

K	K_m	Approach	RTT (s)	Membership (s)	Index (s)	RAM (GB)	Disk (GB)
2^{10}	16	HyDia-CPU-DG	30.60 (1.00 \times)	5.67 \pm 0.08 (1.00 \times)	5.67 \pm 0.24 (1.00 \times)	33.3 \pm 0.1 (1.00 \times)	27.84 \pm 0.00 (1.00 \times)
		BSGS-CPU-DG	13.10 (2.34 \times)	4.92 \pm 0.03 (1.15 \times)	4.76 \pm 0.09 (1.19 \times)	7.2 \pm 0.1 (4.62 \times)	5.52 \pm 0.00 (5.04 \times)
2^{11}	16	HyDia-CPU-DG	30.60 (1.00 \times)	5.72 \pm 0.07 (1.00 \times)	5.49 \pm 0.07 (1.00 \times)	33.3 \pm 0.1 (1.00 \times)	27.84 \pm 0.00 (1.00 \times)
		BSGS-CPU-DG	13.30 (2.30 \times)	4.97 \pm 0.07 (1.15 \times)	4.83 \pm 0.06 (1.14 \times)	7.2 \pm 0.0 (4.62 \times)	5.52 \pm 0.00 (5.04 \times)
2^{12}	32	HyDia-CPU-DG	30.70 (1.00 \times)	5.74 \pm 0.12 (1.00 \times)	5.61 \pm 0.21 (1.00 \times)	33.3 \pm 0.1 (1.00 \times)	27.84 \pm 0.00 (1.00 \times)
		BSGS-CPU-DG	13.30 (2.31 \times)	4.97 \pm 0.06 (1.15 \times)	4.91 \pm 0.31 (1.14 \times)	7.2 \pm 0.1 (4.62 \times)	5.52 \pm 0.00 (5.04 \times)
2^{13}	32	HyDia-CPU-DG	30.70 (1.00 \times)	5.72 \pm 0.09 (1.00 \times)	5.56 \pm 0.12 (1.00 \times)	33.3 \pm 0.1 (1.00 \times)	27.84 \pm 0.00 (1.00 \times)
		BSGS-CPU-DG	13.30 (2.31 \times)	4.98 \pm 0.03 (1.15 \times)	4.82 \pm 0.06 (1.15 \times)	7.2 \pm 0.1 (4.62 \times)	5.52 \pm 0.00 (5.04 \times)
2^{14}	64	HyDia-CPU-DG	30.90 (1.00 \times)	5.68 \pm 0.08 (1.00 \times)	5.52 \pm 0.04 (1.00 \times)	33.4 \pm 0.1 (1.00 \times)	27.84 \pm 0.00 (1.00 \times)
		BSGS-CPU-DG	13.30 (2.32 \times)	4.95 \pm 0.03 (1.15 \times)	4.77 \pm 0.04 (1.16 \times)	7.2 \pm 0.1 (4.64 \times)	5.52 \pm 0.00 (5.04 \times)
2^{15}	64	HyDia-CPU-DG	36.50 (1.00 \times)	7.87 \pm 0.09 (1.00 \times)	7.67 \pm 0.24 (1.00 \times)	33.4 \pm 0.1 (1.00 \times)	30.84 \pm 0.00 (1.00 \times)
		BSGS-CPU-DG	18.70 (1.95 \times)	6.34 \pm 0.09 (1.24 \times)	6.73 \pm 0.68 (1.14 \times)	7.3 \pm 0.0 (4.58 \times)	8.52 \pm 0.00 (3.62 \times)
2^{16}	128	HyDia-CPU-DG	48.40 (1.00 \times)	12.09 \pm 0.29 (1.00 \times)	12.12 \pm 0.38 (1.00 \times)	33.6 \pm 0.2 (1.00 \times)	36.84 \pm 0.00 (1.00 \times)
		BSGS-CPU-DG	27.40 (1.77 \times)	8.94 \pm 0.05 (1.35 \times)	9.55 \pm 0.69 (1.27 \times)	7.4 \pm 0.1 (4.54 \times)	14.52 \pm 0.00 (2.54 \times)
2^{17}	128	HyDia-CPU-DG	77.90 (1.00 \times)	21.91 \pm 0.75 (1.00 \times)	23.54 \pm 0.85 (1.00 \times)	33.9 \pm 0.3 (1.00 \times)	48.85 \pm 0.00 (1.00 \times)
		BSGS-CPU-DG	45.60 (1.71 \times)	14.18 \pm 0.12 (1.55 \times)	16.47 \pm 0.77 (1.43 \times)	7.6 \pm 0.1 (4.46 \times)	26.53 \pm 0.00 (1.84 \times)
2^{18}	256	HyDia-CPU-DG	128.10 (1.00 \times)	39.42 \pm 1.22 (1.00 \times)	41.87 \pm 2.37 (1.00 \times)	34.8 \pm 0.3 (1.00 \times)	72.86 \pm 0.00 (1.00 \times)
		BSGS-CPU-DG	114.10 (1.12 \times)	26.66 \pm 0.47 (1.48 \times)	30.13 \pm 0.30 (1.39 \times)	8.0 \pm 0.1 (4.35 \times)	50.54 \pm 0.00 (1.44 \times)
2^{19}	256	HyDia-CPU-DG	242.20 (1.00 \times)	84.12 \pm 3.38 (1.00 \times)	79.79 \pm 2.25 (1.00 \times)	35.4 \pm 0.3 (1.00 \times)	120.88 \pm 0.00 (1.00 \times)
		BSGS-CPU-DG	173.00 (1.40 \times)	53.64 \pm 0.83 (1.57 \times)	57.91 \pm 0.73 (1.38 \times)	9.0 \pm 0.1 (3.93 \times)	98.57 \pm 0.00 (1.23 \times)
2^{20}	512	HyDia-CPU-DG	483.50 (1.00 \times)	163.66 \pm 3.53 (1.00 \times)	165.61 \pm 3.58 (1.00 \times)	37.3 \pm 0.5 (1.00 \times)	216.93 \pm 0.00 (1.00 \times)
		BSGS-CPU-DG	356.00 (1.36 \times)	112.33 \pm 1.46 (1.46 \times)	115.42 \pm 1.83 (1.43 \times)	11.3 \pm 0.0 (3.30 \times)	194.61 \pm 0.00 (1.11 \times)

Table C.6: CPU/GPU benchmark results with $\kappa = 8$. Values are reported as mean \pm std over 11 trials. The parenthetical value in gray is the ratio against HyDia-CPU-DG as the baseline. GPU rows use an NVIDIA Quadro RTX 8000. For $K = 2^{16}$, HyDia-GPU-DG ran out of GPU memory.

K	K_m	Approach	RTT (s)	Membership (s)	Index (s)	RAM (GB)	Disk (GB)
2 ¹⁰	16	HyDia-CPU-DG	24.90 (1.00×)	4.22 \pm 0.02 (1.00×)	4.04 \pm 0.07 (1.00×)	28.7 \pm 0.0 (1.00×)	24.23 \pm 0.00 (1.00×)
		HyDia-GPU-DG	39.40 (0.63×)	0.63 \pm 0.01 (6.70×)	0.42 \pm 0.00 (9.62×)	24.6 \pm 0.0 (1.17×)	27.23 \pm 0.00 (0.89×)
		BSGS-CPU-DG	10.10 (2.47×)	3.64 \pm 0.04 (1.16×)	3.54 \pm 0.07 (1.14×)	6.1 \pm 0.0 (4.70×)	4.71 \pm 0.00 (5.14×)
		BSGS-GPU-PRS	9.50 (2.62×)	0.25 \pm 0.00 (16.88×)	0.24 \pm 0.00 (16.83×)	3.5 \pm 0.0 (8.20×)	5.61 \pm 0.00 (4.32×)
		BSGS-GPU-PRE	8.50 (2.93×)	0.25 \pm 0.00 (16.88×)	0.24 \pm 0.00 (16.83×)	2.6 \pm 0.0 (11.04×)	4.71 \pm 0.00 (5.14×)
2 ¹¹	16	HyDia-CPU-DG	25.00 (1.00×)	4.21 \pm 0.04 (1.00×)	4.07 \pm 0.08 (1.00×)	28.7 \pm 0.1 (1.00×)	24.23 \pm 0.00 (1.00×)
		HyDia-GPU-DG	39.30 (0.64×)	0.63 \pm 0.02 (6.68×)	0.42 \pm 0.00 (9.69×)	24.6 \pm 0.0 (1.17×)	27.23 \pm 0.00 (0.89×)
		BSGS-CPU-DG	10.10 (2.48×)	3.64 \pm 0.03 (1.16×)	3.56 \pm 0.07 (1.14×)	6.1 \pm 0.0 (4.70×)	4.71 \pm 0.00 (5.14×)
		BSGS-GPU-PRS	9.60 (2.60×)	0.25 \pm 0.00 (16.84×)	0.24 \pm 0.00 (16.96×)	3.5 \pm 0.0 (8.20×)	5.61 \pm 0.00 (4.32×)
		BSGS-GPU-PRE	8.50 (2.94×)	0.26 \pm 0.00 (16.19×)	0.24 \pm 0.00 (16.96×)	2.6 \pm 0.0 (11.04×)	4.71 \pm 0.00 (5.14×)
2 ¹²	32	HyDia-CPU-DG	25.00 (1.00×)	4.26 \pm 0.08 (1.00×)	4.00 \pm 0.11 (1.00×)	28.7 \pm 0.0 (1.00×)	24.23 \pm 0.00 (1.00×)
		HyDia-GPU-DG	39.40 (0.63×)	0.63 \pm 0.01 (6.76×)	0.43 \pm 0.00 (9.30×)	24.6 \pm 0.0 (1.17×)	27.23 \pm 0.00 (0.89×)
		BSGS-CPU-DG	10.50 (2.38×)	3.68 \pm 0.04 (1.16×)	3.60 \pm 0.05 (1.11×)	6.1 \pm 0.0 (4.70×)	4.71 \pm 0.00 (5.14×)
		BSGS-GPU-PRS	9.60 (2.60×)	0.25 \pm 0.00 (17.04×)	0.24 \pm 0.00 (16.67×)	3.5 \pm 0.0 (8.20×)	5.61 \pm 0.00 (4.32×)
		BSGS-GPU-PRE	8.80 (2.84×)	0.25 \pm 0.00 (17.04×)	0.24 \pm 0.00 (16.67×)	2.6 \pm 0.0 (11.04×)	4.71 \pm 0.00 (5.14×)
2 ¹³	32	HyDia-CPU-DG	25.10 (1.00×)	4.24 \pm 0.07 (1.00×)	4.04 \pm 0.09 (1.00×)	28.7 \pm 0.0 (1.00×)	24.23 \pm 0.00 (1.00×)
		HyDia-GPU-DG	39.00 (0.64×)	0.63 \pm 0.01 (6.73×)	0.42 \pm 0.00 (9.62×)	24.6 \pm 0.0 (1.17×)	27.23 \pm 0.00 (0.89×)
		BSGS-CPU-DG	10.30 (2.44×)	3.69 \pm 0.07 (1.15×)	3.61 \pm 0.06 (1.12×)	6.1 \pm 0.0 (4.70×)	4.71 \pm 0.00 (5.14×)
		BSGS-GPU-PRS	9.70 (2.59×)	0.25 \pm 0.00 (16.96×)	0.24 \pm 0.00 (16.83×)	3.5 \pm 0.0 (8.20×)	5.61 \pm 0.00 (4.32×)
		BSGS-GPU-PRE	8.60 (2.92×)	0.25 \pm 0.00 (16.96×)	0.24 \pm 0.00 (16.83×)	2.6 \pm 0.0 (11.04×)	4.71 \pm 0.00 (5.14×)
2 ¹⁴	64	HyDia-CPU-DG	25.10 (1.00×)	4.24 \pm 0.06 (1.00×)	4.02 \pm 0.10 (1.00×)	28.7 \pm 0.1 (1.00×)	24.23 \pm 0.00 (1.00×)
		HyDia-GPU-DG	41.70 (0.60×)	0.63 \pm 0.01 (6.73×)	0.42 \pm 0.00 (9.57×)	24.6 \pm 0.0 (1.17×)	27.23 \pm 0.00 (0.89×)
		BSGS-CPU-DG	10.50 (2.39×)	3.68 \pm 0.08 (1.15×)	3.60 \pm 0.06 (1.12×)	6.1 \pm 0.0 (4.70×)	4.71 \pm 0.00 (5.14×)
		BSGS-GPU-PRS	9.70 (2.59×)	0.25 \pm 0.00 (16.96×)	0.24 \pm 0.00 (16.75×)	3.5 \pm 0.0 (8.20×)	5.61 \pm 0.00 (4.32×)
		BSGS-GPU-PRE	8.70 (2.89×)	0.26 \pm 0.01 (16.31×)	0.24 \pm 0.00 (16.75×)	2.6 \pm 0.0 (11.04×)	4.71 \pm 0.00 (5.14×)
2 ¹⁵	64	HyDia-CPU-DG	29.90 (1.00×)	6.00 \pm 0.12 (1.00×)	5.87 \pm 0.12 (1.00×)	28.7 \pm 0.0 (1.00×)	26.73 \pm 0.00 (1.00×)
		HyDia-GPU-DG	53.00 (0.56×)	1.75 \pm 0.02 (3.43×)	1.66 \pm 0.02 (3.54×)	24.6 \pm 0.0 (1.17×)	30.23 \pm 0.00 (0.88×)
		BSGS-CPU-DG	14.60 (2.05×)	4.85 \pm 0.06 (1.24×)	4.80 \pm 0.14 (1.22×)	6.2 \pm 0.0 (4.63×)	7.21 \pm 0.00 (3.71×)
		BSGS-GPU-PRS	16.80 (1.78×)	0.78 \pm 0.01 (7.69×)	0.81 \pm 0.01 (7.25×)	3.5 \pm 0.0 (8.20×)	8.11 \pm 0.00 (3.30×)
		BSGS-GPU-PRE	15.30 (1.95×)	0.81 \pm 0.01 (7.41×)	0.81 \pm 0.01 (7.25×)	2.6 \pm 0.0 (11.04×)	7.21 \pm 0.00 (3.71×)
2 ¹⁶	128	HyDia-CPU-DG	41.30 (1.00×)	9.71 \pm 0.26 (1.00×)	10.15 \pm 0.61 (1.00×)	28.9 \pm 0.1 (1.00×)	31.74 \pm 0.00 (1.00×)
		BSGS-CPU-DG	22.80 (1.81×)	7.07 \pm 0.08 (1.37×)	7.48 \pm 0.18 (1.36×)	6.3 \pm 0.0 (4.59×)	12.21 \pm 0.00 (2.60×)
		BSGS-GPU-PRS	38.50 (1.07×)	3.02 \pm 0.14 (3.22×)	3.16 \pm 0.05 (3.21×)	4.0 \pm 0.0 (7.22×)	13.11 \pm 0.00 (2.42×)
		BSGS-GPU-PRE	36.10 (1.14×)	3.03 \pm 0.03 (3.20×)	3.13 \pm 0.04 (3.24×)	3.6 \pm 0.0 (8.03×)	12.21 \pm 0.00 (2.60×)
2 ¹⁷	128	HyDia-CPU-DG	64.60 (1.00×)	17.95 \pm 0.58 (1.00×)	17.56 \pm 0.71 (1.00×)	29.1 \pm 0.1 (1.00×)	41.74 \pm 0.00 (1.00×)
		BSGS-CPU-DG	43.30 (1.49×)	11.67 \pm 0.25 (1.54×)	13.53 \pm 0.66 (1.30×)	6.4 \pm 0.1 (4.55×)	22.21 \pm 0.00 (1.88×)
2 ¹⁸	256	HyDia-CPU-DG	130.90 (1.00×)	34.91 \pm 1.31 (1.00×)	35.71 \pm 1.34 (1.00×)	29.8 \pm 0.2 (1.00×)	61.75 \pm 0.00 (1.00×)
		BSGS-CPU-DG	102.50 (1.28×)	22.01 \pm 0.48 (1.59×)	24.64 \pm 0.53 (1.45×)	6.7 \pm 0.1 (4.45×)	42.22 \pm 0.00 (1.46×)
2 ¹⁹	256	HyDia-CPU-DG	200.90 (1.00×)	64.21 \pm 2.92 (1.00×)	63.96 \pm 2.69 (1.00×)	31.3 \pm 0.3 (1.00×)	101.77 \pm 0.00 (1.00×)
		BSGS-CPU-DG	146.90 (1.37×)	44.49 \pm 0.39 (1.44×)	47.09 \pm 0.24 (1.36×)	7.9 \pm 0.1 (3.96×)	82.24 \pm 0.00 (1.24×)
2 ²⁰	512	HyDia-CPU-DG	384.60 (1.00×)	126.35 \pm 3.74 (1.00×)	127.81 \pm 3.96 (1.00×)	34.6 \pm 0.5 (1.00×)	181.81 \pm 0.00 (1.00×)
		BSGS-CPU-DG	306.30 (1.26×)	88.99 \pm 2.70 (1.42×)	95.85 \pm 5.51 (1.33×)	10.1 \pm 0.0 (3.43×)	162.29 \pm 0.00 (1.12×)

- [14] S. Martin, N. Koirala, H. Berens, T. Rozgonyi, M. Brody, T. Jung, Hydia: Fhe-based facial matching with hybrid approximations and diagonalization, Proceedings on Privacy Enhancing Technologies (2025).
- [15] A. A. Badawi, A. Alexandru, J. Bates, F. Bergamaschi, D. B. Cousins, S. Erabelli, N. Genise, S. Halevi, H. Hunt, A. Kim, Y. Lee, Z. Liu, D. Micciancio, C. Pascoe, Y. Polyakov, I. Quah, S. R.V., K. Rohloff, J. Saylor, D. Saponitsky, M. Triplett, V. Vaikuntanathan, V. Zucca, OpenFHE: Open-source fully homomorphic encryption library, Cryptology ePrint Archive, Paper 2022/915, 2022. URL: <https://github.com/openfheorg/openfhe-development>, <https://eprint.iacr.org/2022/915>.
- [16] W. K. Wong, D. W.-l. Cheung, B. Kao, N. Mamoulis, Secure knn computation on encrypted databases, in: Proceedings of the 2009 ACM SIGMOD International Conference on Management of Data, SIGMOD '09, Association for Computing Machinery, New York, NY, USA, 2009, p. 139–152. URL: <https://doi.org/10.1145/1559845.1559862>. doi:10.1145/1559845.1559862.
- [17] H. Hu, J. Xu, C. Ren, B. Choi, Processing private queries over untrusted data cloud through privacy homomorphism, in: 2011 IEEE 27th International Conference on Data Engineering, 2011, pp. 601–612. doi:10.1109/ICDE.2011.5767862.
- [18] Y. Elmehdwi, B. K. Samanthula, W. Jiang, Secure k-nearest neighbor query over encrypted data in outsourced environments, in: 2014 IEEE 30th International Conference on Data Engineering, 2014, pp. 664–675. doi:10.1109/ICDE.2014.6816690.
- [19] F. Li, R. Shin, V. Paxson, Exploring privacy preservation in outsourced k-nearest neighbors with multiple data owners, in: Proceedings of the 2015 ACM Workshop on Cloud Computing Security Workshop, CCSW '15, Association for Computing Machinery, New York, NY, USA, 2015, p. 53–64. URL: <https://doi.org/10.1145/2808425.2808430>. doi:10.1145/2808425.2808430.
- [20] B. K. Samanthula, Y. Elmehdwi, W. Jiang, k-nearest neighbor classification over semantically secure encrypted relational data, IEEE Transactions on Knowledge and Data Engineering 27 (2015) 1261–1273. doi:10.1109/TKDE.2014.2364027.
- [21] H. Shaul, D. Feldman, D. Rus, Secure k -ish nearest neighbors classifier, arXiv preprint arXiv:1801.07301 (2018).
- [22] Z. Brakerski, C. Gentry, V. Vaikuntanathan, (Leveled) fully homomorphic encryption without bootstrapping, ACM Transactions on Computation Theory (TOCT) 6 (2014) 1–36.
- [23] H. Chen, I. Chillotti, Y. Dong, O. Poburinnaya, I. Razenshteyn, M. S. Riazi, {SANNS}: Scaling up secure approximate {k-Nearest} neighbors search, in: 29th USENIX Security Symposium (USENIX Security 20), 2020, pp. 2111–2128.
- [24] M. Zuber, R. Sirdey, Efficient homomorphic evaluation of k-nn classifiers, Proceedings on Privacy Enhancing Technologies (2021).
- [25] Y. Ameer, R. Aziz, V. Audigier, S. Bouzeffrane, Secure and non-interactive k-nn classifier using symmetric fully homomorphic encryption, in: International Conference on Privacy in Statistical Databases, Springer, 2022, pp. 142–154.
- [26] I. Chillotti, N. Gama, M. Georgieva, M. Izabachène, TFHE: Fast fully homomorphic encryption over the torus, Journal of Cryptology 33 (2020) 34–91.
- [27] S. Servan-Schreiber, S. Langowski, S. Devadas, Private approximate nearest neighbor search with sublinear communication, in: 2022 IEEE Symposium on Security and Privacy (SP), IEEE, 2022, pp. 911–929.
- [28] K. Cong, R. Geelen, J. Kang, J. Park, Revisiting oblivious top-k selection with applications to secure k-nn classification, in: International Conference on Selected Areas in Cryptography, Springer, 2024, pp. 3–25.
- [29] I. Ahmad, L. Sarker, D. Agrawal, A. El Abbadi, T. Gupta, Coeus: A system for oblivious document ranking and retrieval, in: Proceedings of the ACM SIGOPS 28th Symposium on Operating Systems Principles, 2021, pp. 672–690.
- [30] J. Fan, F. Vercauteren, Somewhat practical fully homomorphic encryption, Cryptology ePrint

- Archive, Paper 2012/144, 2012. URL: <https://eprint.iacr.org/2012/144>.
- [31] H. Schütze, C. D. Manning, P. Raghavan, Introduction to information retrieval, volume 39, Cambridge University Press Cambridge, 2008.
- [32] A. Henzinger, E. Dauterman, H. Corrigan-Gibbs, N. Zeldovich, Private web search with tiptoe, in: Proceedings of the 29th symposium on operating systems principles, 2023, pp. 396–416.
- [33] H. Asi, F. Boemer, N. Genise, M. H. Mughees, T. Ogilvie, R. Rishi, K. Talwar, K. Tarbe, A. Wadia, R. Zhu, et al., Scalable private search with wally, arXiv preprint arXiv:2406.06761 (2024).
- [34] M. Zhou, E. Shi, G. Fanti, Pacmann: Efficient private approximate nearest neighbor search, Cryptology ePrint Archive (2024).
- [35] M. Zhou, A. Park, W. Zheng, E. Shi, Piano: Extremely simple, single-server pir with sublinear server computation, in: 2024 IEEE Symposium on Security and Privacy (SP), 2024, pp. 4296–4314. doi:10.1109/SP54263.2024.00055.
- [36] X. Wang, M. Zhou, G. De Micheli, Y. Nam, S. Pinge, A. Vega, T. Rosing, Pathe: A privacy-preserving database pattern search platform with homomorphic encryption, in: 2025 IEEE/ACM International Conference On Computer Aided Design (ICCAD), IEEE, 2025, pp. 1–9.
- [37] D. Kim, Y. Nam, W. Wang, H. Gong, I. Bhati, R. Cammarota, T. S. Rosing, M. Tepper, T. L. Willke, Grass: Graph-based similarity search on encrypted query, Cryptology ePrint Archive (2024).
- [38] J. Zhu, L. Patel, M. Zaharia, R. A. Popa, Compass: encrypted semantic search with high accuracy, in: 19th USENIX Symposium on Operating Systems Design and Implementation (OSDI 25), 2025, pp. 915–938.
- [39] V. N. Boddeti, Secure face matching using fully homomorphic encryption, in: 9th IEEE International conference on biometrics theory, applications and systems (BTAS), IEEE, 2018, pp. 1–10.
- [40] J. J. Engelsma, A. K. Jain, V. N. Boddeti, HERS: Homomorphically encrypted representation search, IEEE Transactions on Biometrics, Behavior, and Identity Science 4 (2022) 349–360.
- [41] A. Ibarondo, H. Chabanne, V. Despiegel, M. Önen, Grote: Group testing for privacy-preserving face identification, in: Proceedings of the Thirteenth ACM Conference on Data and Application Security and Privacy, 2023, pp. 117–128.
- [42] H. Choi, J. Kim, C. Song, S. S. Woo, H. Kim, Blind-match: efficient homomorphic encryption-based 1: n matching for privacy-preserving biometric identification, in: Proceedings of the 33rd ACM International Conference on Information and Knowledge Management, 2024, pp. 4423–4430.
- [43] W. Ao, V. N. Boddeti, CryptoFace: End-to-end encrypted face recognition, in: Proceedings of the Computer Vision and Pattern Recognition Conference, 2025, pp. 19197–19206.
- [44] CryptoLab, Cryptolab to participate in rsac 2025, the world’s largest cybersecurity conference “unveiling encrypted facial recognition (efr)”, PR Newswire, 2025. URL: <https://www.prnewswire.com/news-releases/cryptolab-to-participate-in-rsac-2025-the-worlds-largest-cybersecurity-conference-unveiling-encrypted-facial-recognition-efr-302435663.html>, press release. News provided by CryptoLab. Accessed: 2026-03-02.
- [45] CryptoLab, HEaaN2 library, CryptoLab, 2025. URL: <https://cryptolab.gitbook.io/heaan2/>.
- [46] DESILO, The DESILO FHE Library, Documentation, 2026. URL: <https://fhe.desilo.dev/1atest/>.
- [47] W. Choi, J. Kim, J. H. Ahn, Cheddar: A swift fully homomorphic encryption library designed for gpu architectures, in: Proceedings of the 31st ACM International Conference on Architectural Support for Programming Languages and Operating Systems, Volume 1, 2026, pp. 35–49.
- [48] J. H. Cheon, K. Han, A. Kim, M. Kim, Y. Song, Bootstrapping for approximate homomorphic encryption, in: Annual International Conference on the Theory and Applications of Cryptographic Techniques, Springer, 2018, pp. 360–384.
- [49] S. Halevi, V. Shoup, Algorithms in helib, in: J. A. Garay, R. Gennaro (Eds.), Advances in Cryptology – CRYPTO 2014, Springer Berlin Heidelberg, Berlin, Heidelberg, 2014, pp. 554–571.

- [50] J. Deng, J. Guo, N. Xue, S. Zafeiriou, Arcface: Additive angular margin loss for deep face recognition, in: Proceedings of the IEEE/CVF conference on computer vision and pattern recognition, 2019, pp. 4690–4699.
- [51] S. Halevi, V. Shoup, Faster homomorphic linear transformations in helib, in: Annual International Cryptology Conference, Springer, 2018, pp. 93–120.
- [52] J.-P. Bossuat, C. Mouchet, J. Troncoso-Pastoriza, J.-P. Hubaux, Efficient bootstrapping for approximate homomorphic encryption with non-sparse keys, in: A. Canteaut, F.-X. Standaert (Eds.), Advances in Cryptology – EUROCRYPT 2021, Springer International Publishing, Cham, 2021, pp. 587–617.
- [53] J. H. Cheon, D. Kim, D. Kim, Efficient homomorphic comparison methods with optimal complexity, in: International Conference on the Theory and Application of Cryptology and Information Security, Springer, 2020, pp. 221–256.
- [54] Y. Bae, M. Kim, J. Lee, S. Kim, J. Kim, Y. Choi, N. Mireshghallah, Privacy-preserving llm interaction with socratic chain-of-thought reasoning and homomorphically encrypted vector databases, arXiv preprint arXiv:2506.17336 (2025).
- [55] M. S. Paterson, L. J. Stockmeyer, On the number of nonscalar multiplications necessary to evaluate polynomials, SIAM Journal on Computing 2 (1973) 60–66.